Controlling Dislocations to Enable Crystalline Colloidal Robotics

by

Corwin Benedict Kerr

A dissertation submitted in partial fulfillment
of the requirements for the degree of
Doctor of Philosophy
(Chemical Engineering)
in The University of Michigan
2026

Doctoral Committee:

Professor Sharon C. Glotzer, Chair
Professor Albert T. Liu
Professor Abdon Pena-Francesch
Professor Michael J. Solomon

Corwin Benedict Kerr
cbkerr@umich.edu
ORCID iD: 0000-0003-0776-2596

© Corwin Benedict Kerr 2026

DEDICATION

For Dave

ACKNOWLEDGEMENTS

I am very thankful for my advisor, Prof. Sharon Glotzer. Thank you for giving me freedom to try out my ideas, for assembling a great group of people, and for believing that I could be part of that. I'm grateful for my committee, Prof. Albert Liu, Prof. Abdon Pena-Francesch, and Prof. Mike Solomon, for their feedback and encouragement towards bringing out the best story in this work.

A huge thank you to Dr. Philipp Schönhöfer for being so generous with your feedback and advice. Thank you to Karen Coulter, who held us all together. I'm very thankful for Dr. Joshua Anderson for helping us develop practical software. I learned a lot in "code dev" subgroup and from your patient explanations and demonstrations. All the code we wrote and sims we carried out were built on countless hours of donated labor, so I'd like to thank the maintainers and contributors of the free software I used including Emacs, Magit, Python, Jupyter, Numpy, Pandas, Git, FFmpeg, and Slurm.

I thank all the Glotz peeps for contributing to a helpful and friendly atmosphere. I feel very fortunate to have had the early code mentorship of Dr. Bradley and Dr. Vyas. In particular, I thank my cohort Dr. Charlotte, Dr. Tobias, and Dr. Kristi have been very supportive; Dr. Allen for welcoming me to Ann Arbor and for being the de facto lab greeter; Nipuli Gunaratne was a joy to mentor; Dr. Brandon for a wonderful adventure presenting in Germany; Gabby, Trevor, Kate, Isaac, Melody, Zoe, Joseph for fun conversations; and Dr. Ray for support in the final months — we made it! A special thank you to my former roommate and steadfast friend Tobias; you challenged me and helped me grow.

Outside of work, members of the University Musical Society Choral Union, Project Grow gardens, and the Ann Arbor Bicycle Touring Society provided welcome community. Thank you Abdulla for showing me figure skating and pickleball.

I want to thank several mentors at NC State who helped me: Prof. Milad Abolhasani for introducing me to research, Prof Michael Dickey for guidance, and Prof. Larry Blanton for emphasizing the creativity in science. Before that at the Early College at Guilford, Steve Shapiro formed how I approach problems.

Thank you to my family for asking (and asking) about my work, and then asking "is this a colloid?". Mama and Daddy, I ran out of words. Thanks for being there for me. Justin,

good luck wrapping up your PhD. Dave, I found a way through like you said I would! Barb, thanks for keeping us all grounded. Papa, nagyon szeretlek. I wish you could see me now. Leo, you have the distinction of being the only extended family member to visit. Thanks for stopping by on your road trip! Sam, you got me into programming with Scratch and taught me trig. Max, I carry your humor. Steph, Kate, "hive-mind", thanks for the walk chats and support. Chuck, I enjoy having another chemical engineering to talk to. CJ, APS will always remind me of Cirque. Lily, I'm proud of you. To future relatives: You don't have to do a PhD.

Thank you to my partner Areefa for sharing your sense of wonder and supporting me through these years. I love learning things with you. You inspire my creativity and make me a better scientist and person.

TABLE OF CONTENTS

DEDICATION ii

ACKNOWLEDGEMENTS iii

LIST OF FIGURES vii

ABSTRACT viii

CHAPTER

1 Introduction 1

1.1 Colloidal particle building blocks of shape and function 3
1.2 Dislocations in crystals 5
1.3 Traditional computation and control methods 6
1.4 Non-traditional computation 7
1.5 Outline 9

2 Methods and System 10

2.1 System 11
2.1.1 Logic simulations with shear 12
2.2 Visualization and Analysis Methods 14
2.2.1 Voronoi cells and the Delaunay triangulation 14
2.2.2 Identifying dislocations 14
2.2.3 Minimum non-affine squared displacement 15

3 Dislocations by Design: Designing Swelling Clusters to Control Dislocations and Reshape Crystallites 19

3.1 Abstract 19
3.2 Introduction 20
3.3 Methods 21
3.3.1 Simulations 21
3.3.2 Detecting threshold diameter when dislocations first form 21
3.3.3 Tracking most common dislocation motion via heat maps 22
3.3.4 Tracking dislocation direction around asymmetric shapes 23
3.4 Results 23
3.4.1 Effect of cluster side length on dislocation creation (symmetric clusters) 26

3.4.2 Manipulating cluster side length to bias dislocation emission . . . 28
3.4.3 Concave Clusters . . . 33
3.5 Discussion . . . 33
4 Dislocation Logic: Shear Activated Logic Operations in Colloidal Crystals . . . 36
4.1 Abstract . . . 36
4.2 Introduction . . . 37
4.3 Results . . . 39
4.3.1 Dislocation Logic Scheme . . . 40
4.3.2 AND Gate . . . 42
4.3.3 Correctness of the AND Gates . . . 44
4.3.4 NOT Gate . . . 46
4.3.5 Correctness of the NOT gate . . . 47
4.3.6 NAND gate: Sequencing of gates . . . 48
4.3.7 Actuation of the Crystallite: Shear Activated Logic . . . 49
4.4 Discussion . . . 52
5 Conclusion and Outlook . . . 54
BIBLIOGRAPHY . . . 57

LIST OF FIGURES

FIGURE

1.1 Collective robotic systems 3
1.2 Examples of colloidal crystals 3

2.1 Simulation setup 13
2.2 Visualizing dislocations 17
2.3 Localizing dislocations 18

3.1 Previous work on dislocations to reshape crystallites 20
3.2 Dislocation formation patterns around acute and obtuse angled clusters 24
3.3 Dislocations formed around clusters that extend to the edge of the crystallite . 25
3.4 Dislocations formed at different swelling diameters 26
3.5 Thresholds for dislocation emission 29
3.6 Linearized dislocation threshold curve. 30
3.7 Side length biases dislocation direction 31
3.8 Application of swelling cluster design rules 34
3.9 Dislocation paths for hexagon with wedge cutouts 35

4.1 Design of a cluster emitting one dislocation pair 39
4.2 Design and operation of the AND gate 43
4.3 Correctness of the AND gate 45
4.4 Design and operation of the NOT gate 47
4.5 Example failure of the NOT gate 48
4.6 NAND gate from AND and NOT gates 50
4.7 Whole-crystallite view comparing effect of input clusters without AND gate . . 51

5.1 Literature design of a robot made of sliding modules 55

ABSTRACT

Colloidal matter — material made from colloidal particles — holds great promise for achieving robotic-like functionality at microscopic and even nanoscopic length scales. Autonomous sensing, computing, and actuating are essential robotic functions that researchers seek to achieve in particle systems. At millimeter scales and above, electronics make this achievement possible for traditional microrobots. This dissertation explores a novel approach to achieve actuation and computation in systems of identical particles with sizes below a few microns. By engineering the production of defects (specifically, dislocations) in a colloidal crystal monolayer, we show using molecular dynamics simulation how dislocations can be used to change crystal shape and carry out computations, and present design rules that can be applied to experimental systems.

Prior work demonstrated that a cluster of swellable particles embedded within a single layer colloidal crystallite can create dislocations repeatedly with repeating swelling and shrinking cycles, and that it is possible to design the shape of the cluster to achieve macroscopic shape changes of the crystallite. Here we perform a systematic investigation of cluster shape and show how to generate dislocations and emit them along targeted directions to sculpt the crystallite in a desired fashion. We show that acute (60 degree) angle corners of the swelling cluster preferentially emit dislocations, and that, for a given cluster size, there is a threshold for the swollen diameters of the cluster particles above which dislocations form. The direction within the crystallite in which dislocations are emitted can be further tuned by reducing the side length of the cluster below the threshold, including by removing alternating particles from the side. We show that targeted shape changes of the crystallite can be achieved reliably with embedded clusters comprised of particles that

can swell (and shrink) repeatedly by roughly 20%.

Building on these findings, we show how interactions among dislocations in single layer colloidal crystallites can be designed to perform logic operations. We use clusters of swellable particles to create logic gates. We design several logic gates by considering the presence of a dislocation to correspond to logical True, and we apply constant shear to move dislocations (created by swelling a cluster) from input locations on the left to output locations on the right. We construct an AND gate with two embedded clusters arranged symmetrically above and below two input lines to redirect the input dislocations to recombine. We construct a NOT gate by introducing a blocking cluster that prevents a dislocation from moving forward until it can be released by internal recombinations. The NOT gate has three embedded swelling clusters that allow True output when the input is logical False (no dislocation). Finally, we construct a NAND gate from AND + NOT gates by introducing a time delay in the swelling of the clusters. The constructed gates perform correctly roughly 90% of the time. We discuss potential future directions and design improvements towards increasing reliability in real world applications.

CHAPTER 1

Introduction

We usually think of robots as electromechanical machines. However, the word *robot* comes from a play by Karel Čapek, "Rossum's Universal Robots", in which robots were biochemical machines: "colloidal pulp that not even a dog would eat" [1]. Colloids are dispersions of nano- to micro- particles of one phase in another phase with a wide range of properties, like fog (liquid in gas), milk (liquid in liquid), mud (solid in liquid), or opal (solid in solid). The group of particles takes on properties different from the constituents; this emergent behavior means we often think of the whole group as a single substance. By controlling the size, shape, and interactions of the constituent particles, we can design the behavior of the materials [2]. When organized in an ordered crystalline structure, the particles in a colloidal crystal interact with light, resulting in vivid iridescent colors, such as those in Figure 1.2. Stretching a colloidal crystal embedded in polymer can change its color, allowing it be used as a sensor, as shown in Figure 1.2B. There is interest in giving this collective material robotic properties, sometimes called "programmable matter" [3, 4]. Just like colloids with emergent properties, roboticists have explored the ability of swarms of centimeter-scale robots to accomplish tasks as a collective that the individual units cannot [5–10]. For example, "particle robots" (Figure 1.1A) consist of magnetic units that expand and contract. By individually changing the phase offset of the cyclic swelling in response to the distance from a light signal, the collective mass can shuffle towards a target, pass through narrow obstacles, and carry cargo [11]. Kilobots (Fig 1.1B) can form programmed

shapes by local motion and communication [6]. This collective behavior calls to mind the original vision of Čapek of a colloidal material.

Shrinking robots to the micron scale could enable minimally invasive surgery [12], single-cell manipulation [13], or bioremediation [14]. This requires shrinking the sense-compute-act framework of robotic behavior. Richard Feynman called it "infinitesimal machinery" [15]. Roboticists have worked toward shrinking robots with traditional top-down fabrication techniques [16–19], yet at 100s of microns these are not yet colloidal materials.

The emergent collective behavior of colloidal particles inspired an alternative approach to miniaturizing robotic functionality. Different types of particles could be responsible for sensing, carrying out computation, or actuating the robot, contributing their behaviors to the collective assembly [20]. At the particle level, individual particles can "sense" by changing size or shape with exposure to environmental stimuli. Swelling within the crystal strains the crystal and can generate defects, and in particular, dislocations, which are responsible for deforming crystals. If we can control dislocations and bend a crystal from within, we have crystal actuation. However, there is limited work on actuation and computation at the level of the entire colloidal crystal where we see the whole collection as a robot. Controlling a crystalline robot could enable new optical and mechanical programmable materials. The central question of my thesis concerns controlling a crystalline colloidal robot.

In this dissertation, I build on the ability of individual colloidal particles to change their shape as the basis for control and logic in colloidal crystals. The dislocations produced by clusters of swelling particles can actuate a crystallite, and I develop design rules for crystallite shape morphing. The missing link is computing. I identify dislocation recombination rules that can be interpreted as logic operations and use clusters of swelling particles to enact them in model systems. Computing within the crystal using dislocations opens up a way to connect sensing to actuation in a colloidal crystallite. In the future, this operation

could be used to carry out different motions of the crystal in response to different stimuli. My dissertation opens a path to design modular crystalline colloidal robots.

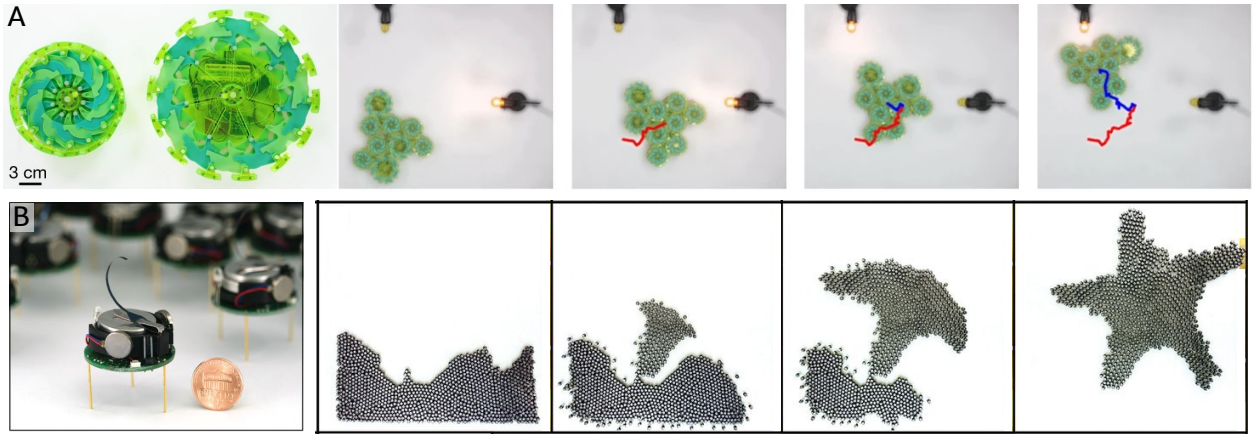


Figure 1.1. Collective robotic systems. (A) Individual particle robots swell and contract and can tune the swelling phase to light intensity. When placed in a mass, the group of particles can move together, something the individuals cannot do. Elapsed time: 30 minutes. Taken from Li et al. [11]. (B) Kilobots move by vibrating their legs. With local communication, a swarm of robotics can form shapes. Elapsed time in image: 12 hours. Taken from Rubenstein et al. [6].

1.1 Colloidal particle building blocks of shape and function

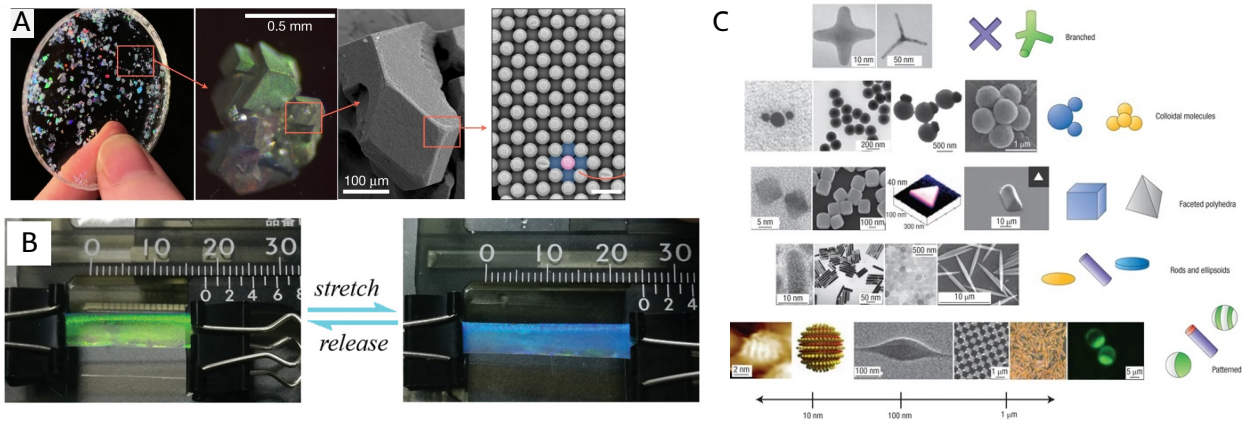


Figure 1.2. Examples of colloidal crystals. (A) A closeup of the ordered structure that interacts with light to produce "structural color". From Hueckel et al. [21]. (B) A colloidal crystal embedded in polymer changes its color when the polymer is stretched. From Liao et al. [22]. (C) Examples of design elements available in colloidal particles. From Glotzer and Solomon [2].

The shape for the robot will be provided by colloidal crystals, which are ordered arrangements made out of colloidal particles. Compared to a disordered blob of matter,

crystals provide structure. The past decades have shown how to design particles that self-assemble into complex colloidal crystal structures. Self-assembly is the process by which nanometer to micron sized particles form ordered structures by minimizing the free energy. The assembly can be designed via particle shape and patchiness, among other design dimensions [2]. The promise of self-assembly is in not having to place every component at the micro or nano scale. Researchers have explored the equilibrium self-assembly of particles with different shapes [2, 23], interactions [21], and stoichiometries [24]. Colloidal crystals bring additional properties to groups of particles, mainly in their interaction with visible and infrared light. Colloidal crystals can be used to sense analytes that change the lattice spacing [22, 25]. In addition to self-assembly, particles can be stamped into groups or formations via carefully-printed templates [26].

Individual colloidal particles can propel via chemical [27] or acoustic propulsion [28]. Collections of such "active" particles have interesting emergent behavior [29, 30]. Propelling particles tend to clump together into writhing masses [31], resulting in motility-induced phase separation. Contact-activated particles can cause the whole swarm to develop traveling waves [32]. Active particles added to a colloidal system can speed up annealing of grain boundaries [33]. External fields can impart energy to control the behavior of colloidal systems [34]. While the field of active matter studies non-equilibrium assemblies or individual particles carrying out tasks, making particles work together to accomplish something is less studied.

Besides propelling, swelling can be seen as another actuation method. Colloidal particles made out of swellable polymers like Poly(N-isopropylacrylamide) (PNIPAm) [35] or liquid crystal elastomers [36] can change their size and shape. Embedding gold nanoparticles into PNIPAm particles can enable localized heating and swelling with light projection [37]. PPy(DBS) (polypyrrole doped with dodecyl benzene sulfonate ions) can swell under an electric potential and has been used for micro-manipulation [13]. When dealing with a particle collective or swarm, a new design dimension emerges from the interaction of

large numbers of components, but control of the collective does not yet extend to crystal arrangements of particles. Control of defects provides this mechanism.

1.2 Dislocations in crystals

Deformation of crystals occurs in discrete steps at the particle level. Each step results from a dislocation. Dislocations exist across crystal length scales, from metals to colloids to bubbles. Dislocations were first demonstrated in bubbles rafts by Bragg and Nye [38]. More recently, colloidal crystals are used to visualize dislocations [39, 40]. Translational symmetry of the crystal remains intact except at the dislocation core. In three dimensions, dislocations exist as lines of interrupted symmetry, and algorithms exist for finding the regions enclosing these lines [41].

Dislocations are commonly described by their Burgers vectors. In an ideal crystal, traversing the crystal lattice in a rectangular path (the "Burgers circuit") brings one back to the starting point. However, attempting a circuit enclosing a dislocation will not connect to the start. The Burgers vector is commonly taken as the vector connecting the start to the finish, known as the SF convention [42], and is conserved within the circuit. If initializing from a perfect crystal (Burgers vector of $\vec{0}$), dislocations form in pairs with opposite Burgers vectors. A dislocation can be thought of as an extra half plane of material wedged into the crystal. Dislocations under shear experience a glide force proportional to the shear projected on the glide plane. The speed is proportional to the force. Dislocations interact under Peach-Koehler forces, with dislocations of opposite Burgers vector attracting each other on their glide plane, and dislocations of like Burgers vector repelling. A dislocation near a free surface is attracted to the surface. The no-traction boundary condition can be modeled as an "image" dislocation of opposite Burgers vector located outside the crystallite, which would attract it. If the dislocation reaches the surface of the crystal, the associated half plane forms a bump on the surface. This means dislocations can be a

tool for reconfiguring the shape of a crystallite. VanSaders explored repeatedly creating dislocations to split an isolated crystallite [43, 44].

Burgers vectors are a useful tool because when dislocations combine, the resultant dislocation has a Burgers vector that is the vector sum of the initial Burgers vectors. The energy of a dislocation is proportional to b^2, where b is the magnitude of the Burgers vector. Not all combinations are favorable, however. If the sum of the squared magnitudes of the Burgers vectors of interacting dislocations would increase, the dislocations will not recombine. This is known as the Frank criterion [45].

There are several experimental techniques for forming and studying dislocations in colloidal crystals. Optical tweezers manipulate intense beams of laser light [46, 47] and are a well-documented method for controlling defects in colloidal crystals [48, 49]. A grain boundary can be seen as regularly-spaced dislocations. Typically, we want to remove defects from crystals by annealing them. Optical tweezers can help anneal grain boundaries [50]. Shear can be used to anneal a crystal [51, 52].

1.3 Traditional computation and control methods

Modern computers use Boolean logic, a model of computation with two states: True and False. Logic gates take one or two inputs and produce an output, which can be connected to more gates. The NOT gate turns input: False into output: True and input: True into output: False. The NAND gate takes two inputs; it outputs True except when both inputs are True. The NOR gate also takes two inputs; it outputs False except when both inputs are False. NAND gates or NOR gates can be combined to produce any other binary logic operation. Transistors can be configured to operate as various logic gates. Complementary metal oxide semiconductor (CMOS) electronics allows billions of transistors to be printed at a time and are the foundation of modern computers.

Recent works in robotics have focused on printing circuits onto particles themselves;

however, the particles produced are larger than the colloidal scale at about 100 microns. Koman et al. used top-down fabrication methods to print simple circuits onto particles that could be used to read environmental signals such as presence of an analyte [16]. Particles were collected to read out information about past environmental exposure. Actuation at the 100 micron scale can be achieved with electrochemical actuators [18] and coupled to CMOS sense and compute units to program walking motions [17]. Integrated circuits can be printed on light-activated colloidal surfers and programmed with light flashing patterns [19]. If scaled down further, particles with onboard electronics could form part of colloidal robots. Another approach is to turn to the collective behavior of a material for computation.

1.4 Non-traditional computation

The first computers were mechanical, like the Babbage difference engine, yet are considered non-traditional today due to the success of silicon electronics [53]. The promise of mechanical computation in general is the native coupling to environmental inputs or outputs. Demonstrating a non-traditional computing method needs a way of encoding the calculation into the physical system, a way for the system to evolve under known rules, and a way to decode the physical result back to the computational result [54]. Logic systems have been made out of bubbles flowing in microfluidic channels [55], origami folds [56], flexible pneumatic tubes [57], mechanical joints and rods [58], and even the collisions of billiard balls [59, 60]. The billiard ball example, in particular, inspired this dissertation (chapter 4) because of its ability to compute with discrete elements.

Non-traditional methods of computation have been achieved with colloidal particles as well. At the collective level, the interactions between particles can be tuned to transfer information. Tanjeem et al. used particles in optical traps to make logic gates [61]. The left-right position of a particle in the trap mapped to True/False, and the spacing between inputs and outputs determined the behavior of the output particle. Lock-and-key colloids

can be used to encode memory in the arrangement of the cluster they form [62]. Colloidal logic has been implemented as the interaction of different system control elements [63], but the inputs and outputs are different entities (inputs: light and pH, outputs: behavior). The clustering behavior of the particles couldn't be turned back into light or pH signal. To be able to connect logic gates together, the inputs and outputs should be the same type.

Work on encoding logic into materials has progressed in simulations of defects in active nematic liquid crystals. Disclinations are a type of defect in 2D systems. Disclinations have been used to make soft robotic actuators that bend [64]. In nematic liquid crystals, disclinations occur at discontinuities in the director field. A common experimental "active nematic" system is formed of microtubules, which provide structure for and help transport material in cells. When polyethylene glycol is added to the system, the depletion interaction causes the microtubules to form bundles of aligned tubes that can form a percolating network. The director field points in the direction that the microtubules are aligned and varies throughout the system. It is almost impossible for all the microtubules in the system to point in the same direction, or even for there to be gradual changes in their direction. Discontinuities in the director field mark the location of disclinations. There are different kinds of disclinations measured by the change in the director field upon encircling the disclination once, but $+1/2$ and $-1/2$ disclinations are common. For a $+1/2$ disclination, the director field changes by 180 degrees while circling the disclination. For a $-1/2$ disclination, the director field changes by -180 degrees.

In cells, kinesin motor proteins transport materials along the microtubule network. When added to the bundles of microtubules, the kinesin motor proteins cause the microtubules to slide among one another [65]. At the quasi-2D, oil-water interface, $+1/2$ disclinations are driven throughout the system resulting in a continuous churning motion. The activity can be controlled by varying the concentration of ATP, the fuel for the kinesin. By using a modified myosin protein instead of kinesin, the activity can be made sensitive to light, and therefore able to be patterned optically [66]. This is what inspired previous work to take

on the control of defects. Previous work has used disclinations as logic carriers for logic operations [67] and Boolean logic gates [68].

1.5 Outline

My dissertation focuses on controlling the formation and migration of dislocations to impart robotic functions to colloidal crystalline materials. I create dislocations in my simulated crystal by embedding a cluster of cyclically swelling and shrinking particles in the crystal.

Chapter 2 describes simulation and analysis methods.

In Chapter 3, I investigate the geometry of the cluster to generate design rules for more precise control over dislocation formation and motion. I decompose the geometry of the cluster of swelling particles into basic elements such as angle, side length, and cluster asymmetry and show that these geometric elements dictate dislocation formation and migration within the 2D crystallite. Above a certain threshold, dislocations form and emit from acute angles, allowing for the design of shape changes of the crystallite.

In Chapter 4, I use dislocations to carry out Boolean logic operations within the crystal. I map the presence of a dislocation to logical True, then position swelling clusters of particles to create input dislocations and internal dislocations. I design configurations such that recombinations of the dislocations can map to AND, NOT, or NAND gates, the latter showing that multiple gates can be sequenced together, albeit requiring staged swelling cycles.

Chapter 5 concludes with ideas for future work.

CHAPTER 2

Methods and System

To study the behavior of clusters of swellable particles within a colloidal crystallite, we perform molecular dynamics simulations. Colloidal particles experience kicks of force from molecules in the surrounding solvent, resulting in Brownian motion, which can be modeled as a random process. In simulation, this is achieved by applying a random force to each particle. We assume an underdamped system where particle inertia matters, hence we model the particle motion via Langevin equation of motion:

$$m\frac{d\vec{v}}{dt} = \vec{F}_C - \gamma \cdot \vec{v} + \vec{F}_R \tag{2.1}$$

where m is particle mass, $\vec{v}$ is particle velocity, $\vec{F}_R$ is a uniform random force (with $\langle \vec{F}_R \rangle = \vec{0}$ and $\langle \|\vec{F}_R\|^2 \rangle = 4kT\gamma/\delta t$) modeling Brownian motion with drag coefficient γ, and $\vec{F}_C$ is the conservative force due to interaction with other particles. This force is due to pairwise interparticle potentials $V_{ij}(r)$ and external shear field F_{shear} (for Chapter 4) $\vec{F}_C = \sum_{ij} \frac{-\partial Vij}{\partial r_{ij}} + F_{shear}$, both of which we detail below. The simulations were performed at $k_BT = 0.2$ using $m = 10$, $\gamma = 1$ and simulation step size $\delta t = 0.005$. We carry out two dimensional molecular dynamics simulations in HOOMD-blue, versions 4-5 [69–71].

2.1 System

We initialize a hexagonal lattice of particles, spaced apart by their diameters $a_{init} = 1$, then delete particles outside a circle of radius $R_{crystallite}$, as shown in Figure 2.1B. For Chapter 3, $R_{crystallite} = 40a_{init}$ (yielding $33\,000$ particles in the simulation). For Chapter 4, $R_{crystallite} = 250a_{init}$ ($226\,679$ particles). The simulation is conducted in a box with periodic boundary conditions much larger than the size of the crystallite so that the crystallite does not wrap around the boundary.

The simulation consists of two particle types: passive particles and swelling particles. The swelling particles are arranged in a fixed pattern at the center of the crystallite forming what we call the cluster. The number of particles in the cluster ranges from 3 to 1141 depending on the cluster shape.

The diameter $a(t)$ of the swelling particles changes over time with a cyclic function shown in Figure 2.1C using the HOOMD-blue Cycle variant.

$$a(t) = \begin{cases} a_{init} & x < t_A \\ a_{init} + r(x - t_1) & t_1 < x < t_2 \\ a_{max} & t_2 < x < t_3 \\ a_{max} - r(x - t_3) & t_3 < x < t_4 \end{cases} \tag{2.2}$$

where $x = mod(t, t_A + t_{AB} + t_B + t_{BA})$, r is the swelling rate, $t_{AB} = t_{BA} = \frac{a_{max} - a_{init}}{r}$, $t_1 = t_A$, $t_2 = t_1 + t_{AB}$, $t_3 = t_2 + t_B$, and $t_4 = t_3 + t_{BA}$. We use $t_A = t_B = 50000$.

Swelling particles are harmonically bonded to neighbor swelling particles per Equation 2.3.

$$V_{ij}(r) = \frac{1}{2}k(r_{ij} - r_0)^2 \tag{2.3}$$

with rest length $r_0 = a(t)$, matching the diameter, and spring constant $k = 100$. This prevents the motion of dislocations from dispersing the particles in the cluster, so we can treat the swelling cluster as a single object rather than individual particles.

Particles interact under a Lennard-Jones potential [72] with

$$V_{ij}(r) = \begin{cases} 4\epsilon\left[\left(\frac{\sigma}{r_{ij}-\Delta_{ij}}\right)^{12} - \left(\frac{\sigma}{r_{ij}-\Delta_{ij}}\right)^{6}\right] - 4\epsilon\left[\left(\frac{\sigma}{r_{cut}-\Delta_{ij}}\right)^{12} - \left(\frac{\sigma}{r_{cut}-\Delta_{ij}}\right)^{6}\right] & r \leq r_{cut} \\ 0 & r > r_{cut} \end{cases} \tag{2.4}$$

The second term in equation 2.4 shifts the potential to 0 after a cutoff radius $r_{cut} = 3$ to reduce the number of pairwise interactions that need to be computed.

The current diameter of the particles sets the per-pair Δ_{ij} from the interacting pairwise diameters:

$$\Delta_{ij} = \frac{1}{2}\left(a_i + a_j\right) - a_{init} \tag{2.5}$$

Figure 2.1A plots the pair potential between a passive particle and a swelling particle.

We use $\epsilon = 10k_bT$ because it creates a robust crystallite that does not fracture, yet has enough surface tension to maintain its boundary and minimize the appearance of voids upon shrinking of the cluster. We use $\sigma = 2^{-1/6}a_{init}$, so when $a_i = a_j = a_{init}$, $\Delta_{ij} = 0$, and the potential energy minimum occurs at $r = 2^{1/6}\sigma = a_{init}$.

The diameter of the swelling particles follows a cyclic sloped step function (Fig 2.1C). For Chapter 3, the swelling rate for dislocation density simulations is $1 \times 10^{-6}\,\mathrm{a_{init}}\delta\mathrm{t}^{-1}$ and $5 \times 10^{-7}\,\mathrm{a_{init}}\delta\mathrm{t}^{-1}$ for threshold simulations. The diameter updates every $100\delta t$ timesteps.

2.1.1 Logic simulations with shear

We initialize a hexagonal lattice of particles, spaced a unit distance apart, then delete particles outside a circle of radius 250 particles, leaving 226,679 particles in the crystal.

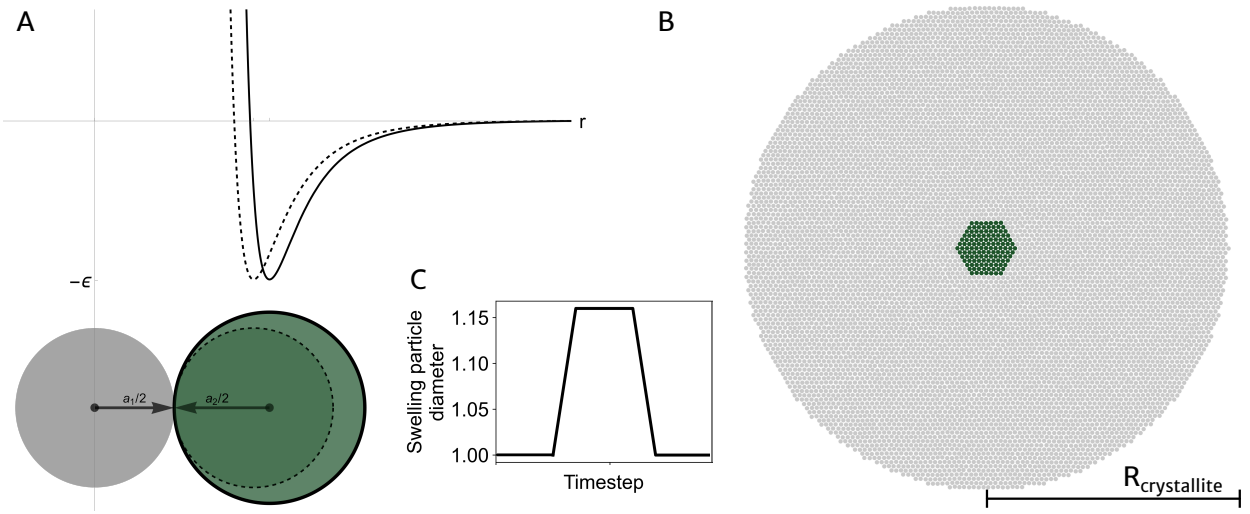


Figure 2.1. Simulation setup. (A) The pair potential used to simulate particle interactions. Below, the gray particle has radius a_1, and the green particle has radius a_2. The dashed circle represents $a_2 = a_1$ and corresponds to the dashed line on the plot. The solid line shows the pair potential when $a_2 > a_1$. The minimum of the potential occurs at the equilibrium separation of the particles $\frac{1}{2}(a_1 + a_2)$. (B) The crystallite containing a cluster, shown in green. The radius of the crystallite is $R_{crystallite}$. (C) Example swelling profile of the swelling particles.

We anneal the simulation for 1000 timesteps using NVT simulation with the Bussi thermostat [73] as we ramp kT from 0.001 to 0.03. We switch to Langevin dynamics (Equation 2.1) for the rest of the simulation with $\gamma = 1$, $kT = 0.2$, $m = 1$.

For the single-gate simulations (AND and NOT), the cluster particle diameter increases from 1 to 1.14 over 2000 timesteps, is held at 1.14 for 100,000 timesteps, then shrinks back to 1 over 2000 timesteps. The swelling rate is $7 \times 10^{-5}\,\mathrm{a_{init}\delta t^{-1}}$ to reduce simulation time. The diameter updates every $100\delta t$. For the NAND gate simulations, the cycles are the same, but the NOT cycle is delayed by $105,000$ timesteps from that of the AND gate cycle.

We apply a global shear force $\vec{F}_{shear}$ to the crystal to propel dislocations by applying a horizontal force to each particle that varies with the vertical coordinate: $\vec{F}_{shear} = (my, 0)$. The shear factor for the AND and NOT simulations is $m = 1 \times 10^{-4}$. The shear in the NAND simulations is $m = 5 \times 10^{-5}$.

2.2 Visualization and Analysis Methods

Within a given region of crystal, the total measure of dislocations (the Burgers vector) is conserved, but if a dislocation reaches the surface, the deformation transmitted by the dislocation manifests as a bump on the surface (Figure 2.2A). We introduce a reliable method to track dislocations during simulations based on Voronoi diagrams and particle displacements.

2.2.1 Voronoi cells and the Delaunay triangulation

The Voronoi cell decomposition of a system consists of cells that partition space into regions nearest each particle [75]. It can be used to highlight dislocations in a crystal lattice (Figure 2.2C). For example, in a perfect hexagonal lattice, the Voronoi cell decomposition yields a hexagon around each particle, tiling space. At the dislocation, however, a pentagon–heptagon pair (5–7 pair) appears in the Voronoi decomposition among the hexagons. This is a useful method for tracking dislocations as they move.

As the dual of the Voronoi decomposition, the Delaunay triangulation (Figure 2.2D) can be derived from the Voronoi decomposition by connecting points whose Voronoi cells share a boundary. The number of edges emanating from a point can be taken as the number of neighbors of that particle. The edges of the Delaunay triangulation can be seen as steps along the Burgers circuit in determining the Burgers vector.

2.2.2 Identifying dislocations

To localize dislocations to the nearest triangle, we match each triangle edge to the nearest lattice direction and compute the sum around each triangle. The sum is the Burgers vector of that region of crystal, which we take as the presence of a dislocation when it is non-zero. We implemented a near real-time 2D version of this algorithm described by Stukowski (see Figure 2.3) [76]. The current implementation assumes that the lattice is oriented with

the main lattice vectors parallel to the horizontal axis. The boundary of the crystallite presents a problem for the algorithm due to the elongated Delaunay triangles. We use an implementation that filters out these long triangles to avoid false positives at the crystallite boundary. The algorithm is visualized in Figure 2.3.

2.2.3 Minimum non-affine squared displacement

In addition to identifying the position of dislocations on a single frame, we want to be able to identify the paths of deformation left by a passing dislocation given two frames. Elastic deformation (combination of scaling and shearing) can be described by an affine transformation, a matrix transformation that preserves parallel lines. Purely affine transformation models the elastic displacement of particles tracked between the frames (Figure 2.2E). Any transformation in particle positions that cannot be captured by an affine transformation is indicative of particle rearrangements. In our case of a crystal lattice, particle rearrangements are almost always due to the passage of a dislocation. Brief appearances of voids are rare. The amount of deformation can be tracked by how "non-affine" it is.

Falk and Langer formalized this parameter, the minimum non-affine squared displacement D^2_{min}, in a study of particle rearrangement in amorphous structures [77]. Let t be the time of the current frame and $t - \Delta t$ be the time of the reference frame. For neighbor particles notated n within a cutoff radius ($n = 0$ is reference particle) having positions r_n with superscript i or j coordinate indices, the mean squared difference between the displacement of neighbor particles to the reference particle and the displacement of neighbor particles to the reference particle under affine strain is:

$$D^2(t, \Delta t) = \sum_n \sum_i \left(r^i_n(t) - r^i_0(t) - \sum_j (\delta_{ij} + \epsilon_{ij}) \times [r^j_n(t - \Delta t) - r^j_0(t - \Delta t)] \right)^2 \tag{2.6}$$

where ϵ_{ij} is the strain in the neighbor region.

To find the minimum strain, Falk and Langer determine:

$$X_{ij} = \sum_n [r_n^i(t) - r_0^i(t)] \times [r_n^j(t - \Delta t) - r_0^j(t - \Delta t)] \tag{2.7}$$

$$Y_{ij} = \sum_n [r_n^i(t - \Delta t) - r_0^i(t - \Delta t)] \times [r_n^j(t - \Delta t) - r_0^j(t - \Delta t)] \tag{2.8}$$

$$\epsilon_{ij} = \sum_k X_{ik} Y_{jk}^{-1} - \delta_{ij} \tag{2.9}$$

Minimizing strain then gives the minimum non-affine squared displacement D^2_{min}.

We use the method as implemented in the Atomic Strain modifier of the Ovito visualization and analysis tool, version 3.12.0 [78, 79]. Ovito does not normalize the value, so it increases with an increasing cutoff radius. We use cutoff radius of 1.8 particle diameters.

For visualization, the reference frame is the first frame of the simulation. Figure 2.2E shows the particles around a dislocation colored by their D^2_{min}. For heat maps, the reference frame is the frame before swelling begins. To select particles near dislocation paths we use a threshold $D^2_{min} > D^2_{min,thresh} = 2$, having found that this selects 1-2 particle layers around the glide plane.

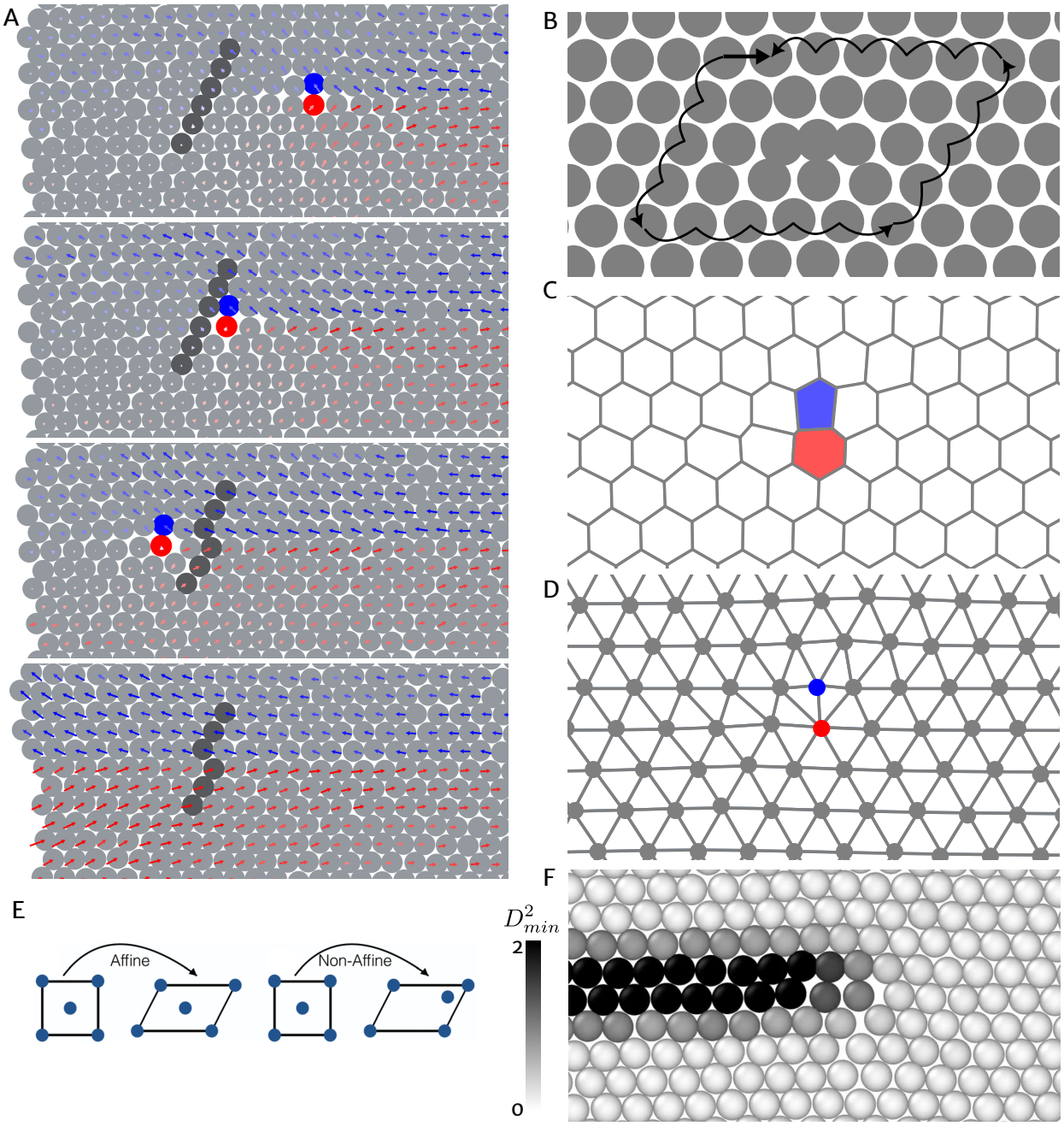


Figure 2.2. Visualizing dislocations. (A) A dislocation (red-blue particles) moves to the left and displaces the surface. Dark gray particles are to guide the eye. Each particle is annotated with its displacement vector, colored red-blue by the magnitude of the displacement in the x direction. (B) Determining the Burgers vector of a dislocation. A right-hand 4×5 Burgers circuit is constructed, and the Burgers vector $\vec{b}$ is the vector from the start to the end of the Burgers circuit. Here, $\vec{b} = (1, 0)$. (C) The Voronoi cell decomposition of the particles containing the dislocation above. The blue cell is 5-sided. The red cell is 7-sided. (D) The Delaunay triangulation of the particles containing the dislocation above. (E) Illustration of affine vs non-affine deformation, taken from Ganguly et al. [74]. (F) Particles colored by minimum non-affine squared displacement (colorbar inset) of a $(1, 0)$ dislocation moving from left to right.

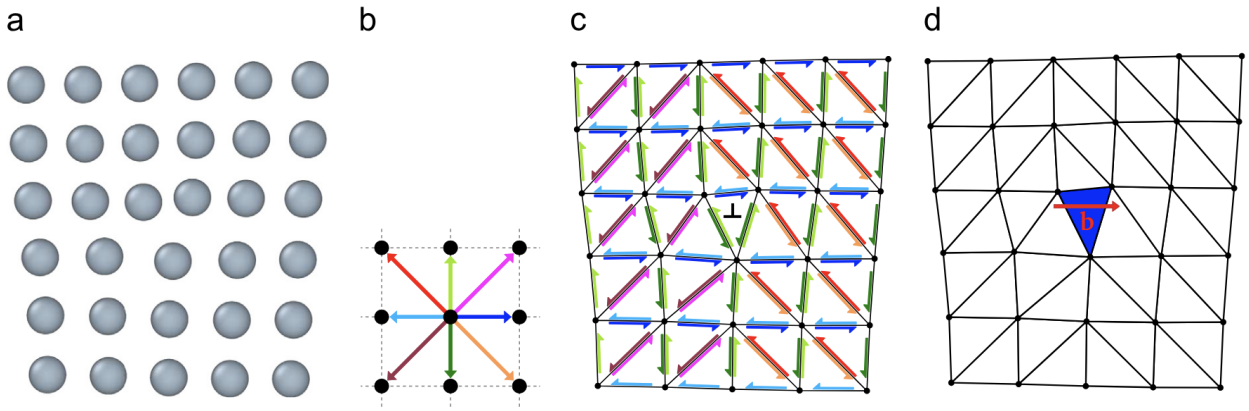


Figure 2.3. Localizing dislocations, described by Alexander Stukowski [76]. (A) Particle positions. (B) ideal crystal vectors. (C) Delaunay triangulation. (D) The ideal vectors fail to close at the location of the dislocation. From [76].

CHAPTER 3

Dislocations by Design: Designing Swelling Clusters to Control Dislocations and Reshape Crystallites

3.1 Abstract

Robots comprised of collections of colloidal particles could perform targeted tasks such as collective morphological changes on the micron scale; however, no such robot has been made out of a colloidal crystal due to the difficulty of precisely controlling particle motion in the confined environment of a crystal. To create dislocations that carry shear deformation, we simulate a cluster of cyclically swelling and shrinking colloids implanted into a finite 2D colloidal crystallite. We find that acute angles of the cluster preferentially emit dislocations, and that there is a swelling threshold above which dislocations form. Cluster sides brought below the threshold by shortening or perforating them do not emit dislocations, providing a way to bias dislocation emission with asymmetric cluster shapes. Targeted dislocations can reshape the boundary of an isolated colloidal crystal. This work paves the way to design intricate morphological changes of colloidal crystallites, towards making a shape-changing machine for manipulating microscale objects.

3.2 Introduction

Self-assembly of colloidal crystals has shown promise in precisely positioning particles on the nano- to micro- scale to achieve targeted global properties [2]. Imparting reconfigurability to a crystal at that scale could allow for a new class of self-healing or robotic materials. In crystals, reconfiguration without fully re-assembling the structure requires controlling plastic deformation, namely, the creation and migration of dislocations.

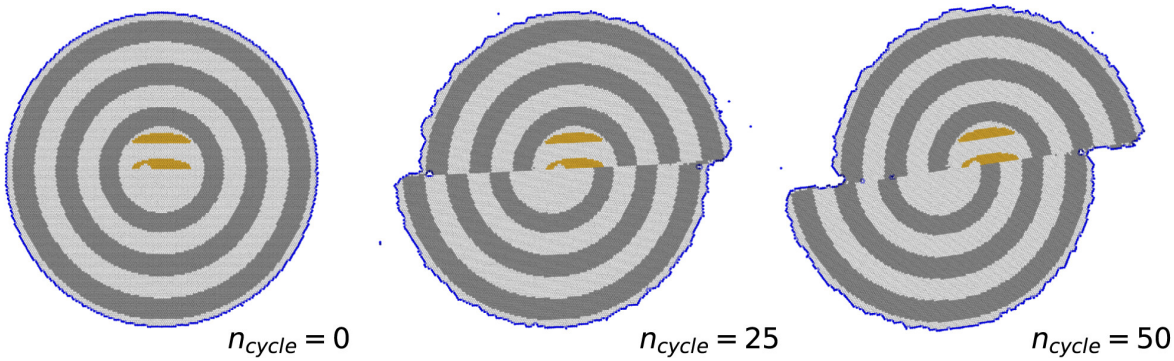


Figure 3.1. Previous work on dislocations to reshape crystallites. Top down view of 2D simulation. The yellow particles swell and shrink. After 50 swell-shrink cycles, the crystallite is sheared in half along the glide plane of the dislocations emitted by the bottom half-ellipse cluster. Gray colors are to guide the eye. Blue particles are low density particles at the edge. Taken from VanSaders and Glotzer [43].

Previous work demonstrated a promising method to reshape a 2D crystal by harnessing dislocations created around clusters of swelling particles [43, 44]. Cyclic swelling and shrinking of an intuitively-designed cluster of particles creates dislocation pairs that emit towards opposite sides of the crystallite. Each dislocation moves until it interacts with another dislocation or reaches the surface. Clusters were made of two half ellipses with a notch cut out of the lower one. The offset of the notch caused a repeatable splitting of the dislocation pair that could split the crystallite in half, as shown in Figure 3.1. Even though the cluster emitted dislocations, the specific features of the cluster shape were not investigated in detail, making it difficult to design new clusters that reshape the crystallite differently. More complex shape changes would be possible if dislocations are generated and emitted in sequence. However, it remains unclear how to design the shape of the

embedded cluster of swelling particles to create the desired dislocations in terms of Burgers vector and propagation direction.

Here, we present design rules for controlling the creation and emission of dislocations based on a systematic study of the effects of cluster features on the dislocations they emit. We show how side lengths and corner angles together define where dislocations form. We show that a 60° corner in a cluster is preferred for creating dislocation pairs. We determine the threshold at which we have control over dislocations with an eye towards experiments with swelling particles. We find that clusters with roughly 5 particles per side were able to generate dislocations if the particles can swell by at least 20%. Finally, we extend the design rules to control the direction of dislocation emission via asymmetric cluster geometries.

3.3 Methods

3.3.1 Simulations

All simulations were performed with Langevin dynamics molecular dynamics simulations in HOOMD-blue as described in Section 2.1.

3.3.2 Detecting threshold diameter when dislocations first form

To find the particle diameter threshold a_{T} for the cluster to emit dislocations, we performed simulations of one swell-shrink cycle for various maximum diameters a_{max} and side lengths s and determined the number of dislocations formed at the peak of the cycle. We gradually swelled and shrank symmetric convex cluster shapes (triangle, hexagon, parallelogram), holding the swelling rate constant at $5\times10^{-7}\,\mathrm{a_{init}}\delta\mathrm{t}^{-1}$. To count dislocations in a simulation frame, we compute the Voronoi decomposition of the particle positions within a circle of radius $R_{crystallite} - 3$, where $R_{crystallite}$ is the number of particles that make up the crystallite radius, using SCIPY [80]. We take the number of 5-coordinated

Voronoi cells as the number of dislocations, after confirming that it matches the number of 7-coordinated Voronoi cells.

We ran 30 replicate simulations with different random seeds and computed error bars as the standard deviation. These swelling plots are shown in Figure 3.4. We draw a horizontal line "cutoff line" on the swelling plot at 0.5, representing over half of the simulations of that cluster type that nucleated dislocations. The smallest diameter value that intersects this line is the threshold a_T.

To propagate the error from the vertical direction (maximum dislocations) to the threshold in the horizontal direction (maximum diameter of cluster), we use the following algorithm of overlapping error bars: The value for the threshold plot could conceivably be any of the nearby points whose error bars overlap the cutoff line. We take the maximum interval that encompasses all points whose error bars cross the threshold value as the error interval for the cluster diameter threshold.

3.3.3 Tracking most common dislocation motion via heat maps

We represent the aggregate motion of dislocations across replicate simulations using heat maps of particles disturbed by passage of a dislocation. We compute the per-particle minimum non-affine squared displacement D^2_{min}(see Section 2.2.3) for simulation frames corresponding to the beginning and top of the swelling cycle for each cycle (5 cycles) in the simulation (10 simulations) using a maximum diameter $a_{max} = 1.18a_{init}$. We select particles with $D^2_{min} > D^2_{min,thresh}$ as being near dislocation paths and found that $D^2_{min,thresh} = 2$ selected the nearest 1-2 particles. We aggregate the positions of these particles across all cycles and simulations and bin their positions on a hexagonal grid. The "hottest" parts of the heat map correspond to locations of particles interrupted by one dislocation per cycle. For the heat map simulations, we use a fixed swelling rate of $1 \times 10^{-6}\,\mathrm{a_{init}}\delta\mathrm{t}^{-1}$. The faster swelling rate does not affect the direction that dislocations emit, so it does not affect the heat maps. We use dwell times of $t_A = t_B = 20000$ timesteps.

3.3.4 Tracking dislocation direction around asymmetric shapes

We sequentially shortened one side of a parallelogram cluster from a 9×10 parallelogram to a 4×10 parallelogram and carried out swell-shrink simulations with 5 cycles each for 100 replicas.

In addition to creating heat maps as described in the previous section, we count dislocations that travel in each crystal direction. For each cycle of each simulation, we divide particles satisfying $D^2_{min} > D^2_{min,thresh}$ into groups of particles using the analysis package FREUD [81]. For each group, we fit a line to the particle x, y coordinates. The direction of the corresponding dislocation is determined by binning the slope of the line into $60°$ angular bins around each direction.

3.4 Results

The number of dislocations formed in one swell-shrink cycle depends on the cluster shape, the number of particles forming a side of the cluster s, and the maximum diameter of swelling particles a_{max}. The shape of any connected cluster of particles embedded in our crystallite can be formed of angles that are multiples of 60 degrees, which are compatible with the crystal orientations of the hexagonal crystal: the convex angles $60°$ (*acute*) and $120°$ (*obtuse*) as well as interior (concave) angles $240°$ and $300°$. Convex shapes enable the dislocation pair to split and travel along a glide plane, whereas concave shapes only allow one half of the dislocation pair to emit. Thus, we first study clusters with the three simplest convex shapes with equal side lengths: triangle, parallelogram, and hexagon.

Figures 3.2(A-B) show how dislocation pairs form at corners, and 3.2C shows typical patterns of dislocation emission around clusters. Each corner emits a dislocation with the 7-coordinated particle on the outside (with respect to the cluster) of the glide plane. Figure 3.2D shows heat maps that illustrate the most common direction of dislocations around the clusters. The triangle and hexagon clusters emit dislocations on all corners. For

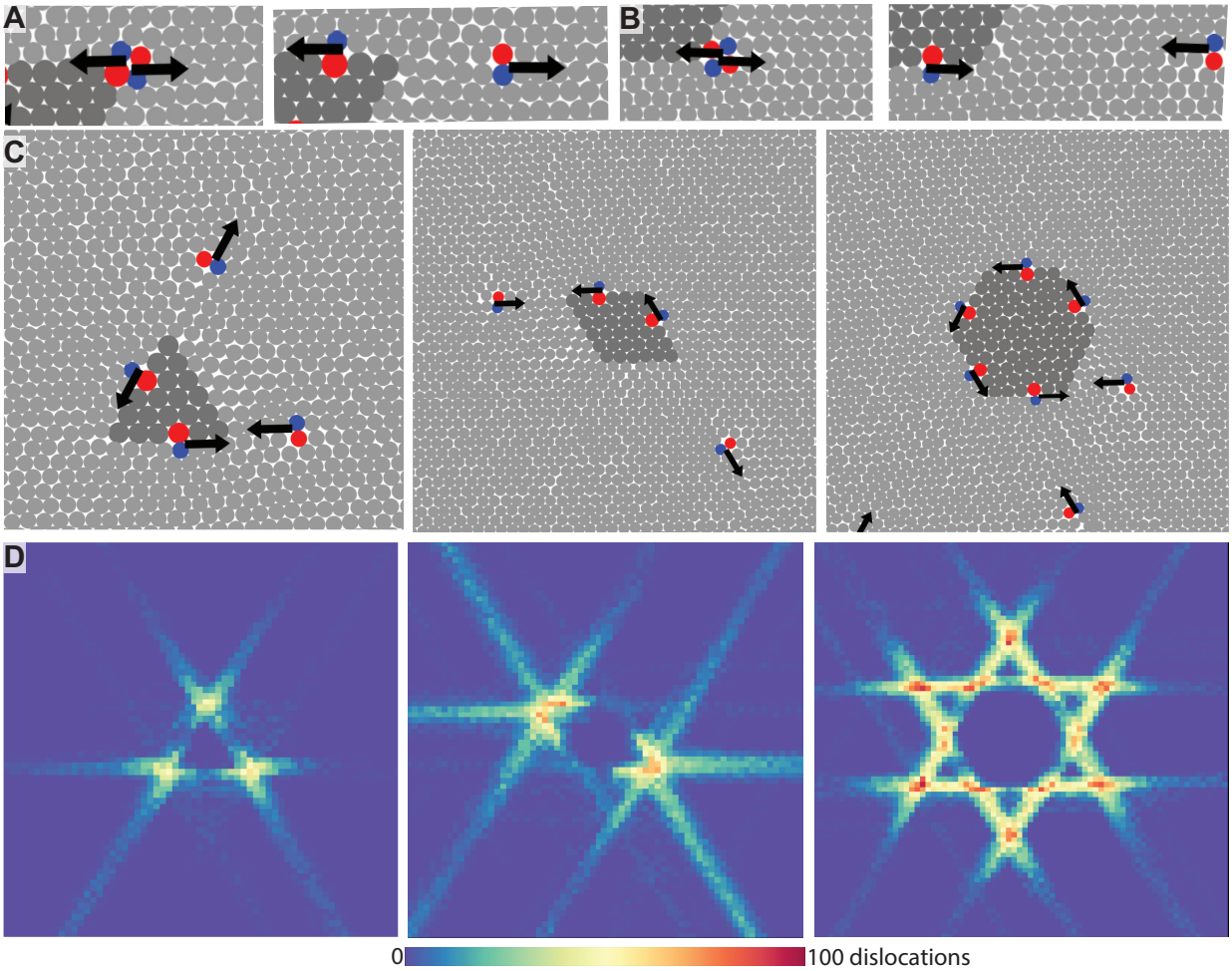


Figure 3.2. Dislocation formation patterns around acute and obtuse angled clusters. **(A)** Acute angle forming a dislocation pair. **(B)** Obtuse angle forming a dislocation pair. **(C)** Simulation snapshots near the end of a swelling cycle for triangle, parallelogram, and hexagon clusters of $s = 6$. Swelling particles are shown in darker gray. Red/blue particles have 7/5 neighbors. Dislocation Burgers vectors are shown as black arrows and are magnified by roughly a factor of 3 for ease of viewing. **(D)** Aggregate motion of dislocations, shown as heat maps of particles disrupted by plastic deformation. Images show 10 replicate simulations of 5 swelling cycles for clusters with 8 particles per side. The color bar is the number of times a particle was near a passing dislocation.

the hexagon cluster, the 6-fold symmetry means that after the first dislocations emit, upon shrinking the hexagon emits dislocations that form a grain boundary loop, which results in the the hexagon cluster being slightly rotated within the crystallite [49]. Swelling the hexagon cluster is therefore a way to convert linear swelling motion of the particles into rotation of the cluster. For the parallelogram cluster shapes, many dislocations move away along glide planes not parallel to any adjacent sides of the cluster. These dislocations result from the recombination of dislocations that form on adjacent sides and are explored more in Chapter 4.

The parallelogram creates only two dislocation pairs at the acute corners at its threshold, then creates two more pairs at the obtuse angled corner when the cluster particles swell to a larger diameter. This behavior suggests that the particles must swell to a different diameter threshold to emit dislocations at an acute *vs.* at an obtuse corner. We test this hypothesis by swelling corners of clusters that extend to the boundary of the crystallite to isolate the effect of the corner.

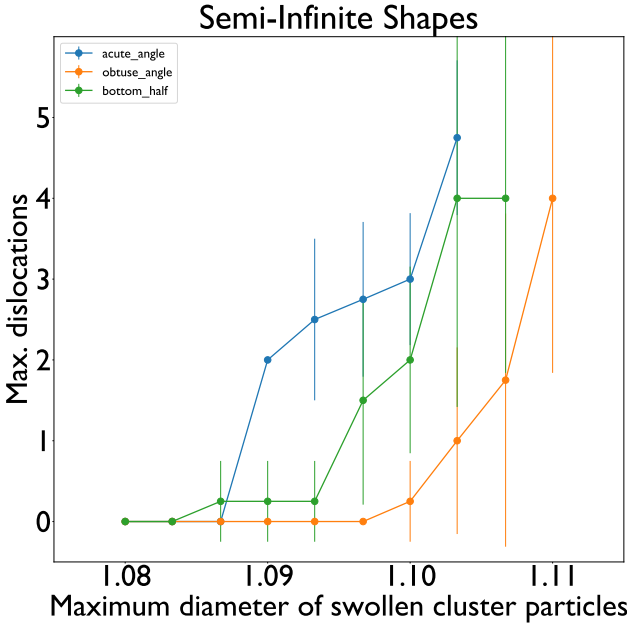


Figure 3.3. Dislocations formed around clusters that extend to the edge of the crystallite. The acute angled corner creates dislocations at the smallest swollen diameter.

To estimate the diameter threshold for clusters formed of an angle extending to the edge

of the crystallite, we construct swelling clusters out of particles in the circular crystallite ($R_{crystallite} = 40$) that satisfy: For the half cluster: $p_y < 0$. For the acute angle: $p_y < p_x * \tan 60°$ and $p_y < p_x * \tan -60°$. For the obtuse angle: $p_y < p_x * \tan 60°$ and $p_y < 0$ where p_x and p_y are the x and y positions of a given particle. We produce a "swelling plot", shown in Figure 3.3, as described in Section 3.3.2 and estimate the threshold with a cutoff of 0.5 dislocations. We find that the acute corner emits dislocations before the obtuse corner (Table 3.1).

Table 3.1. The thresholds for different angle clusters that extend to the edge of the crystallite.

Cluster type	Threshold
Acute	1.090
Obtuse	1.103
Half-plane	1.097

3.4.1 Effect of cluster side length on dislocation creation (symmetric clusters)

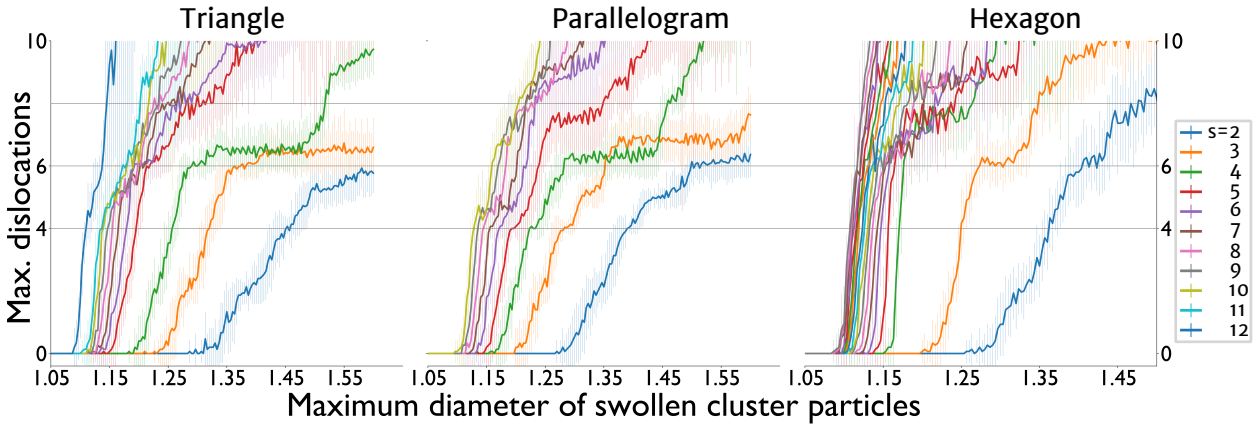


Figure 3.4. Dislocations formed at different swelling diameters. Number of dislocations formed around swelling clusters vs swollen diameter of particles in the cluster for triangle, parallelogram, and hexagon cluster shapes. Side length s=2 through 20.

For finite clusters, Figure 3.4 shows the number of dislocations formed around cluster particles that swell to different diameters for different sized clusters. Consider a cluster

with side length $s = 6$. When a_{max} is small ($a_{max} \lessapprox 1.13a$), no dislocations form. As a_{max} approaches $1.15a$, dislocation pairs transiently appear and disappear at the corners. At a certain diameter, dislocation pairs form on the corners. We term this value of a_{max} the diameter threshold a_T. When $a_{max} \gtrapprox a_T$, the dislocation pairs begin to separate, traveling along glide planes parallel to the sides of the cluster. When the dislocation pairs separate, one dislocation glides away parallel to its side of the cluster, and the other one remains stuck to the cluster side. If the cluster particles swell past the emission threshold, additional dislocation pairs form, emit, and react with each other, resulting in dislocations traveling in directions unrelated to the directions of the cluster sides. As the cluster subsequently shrinks, the stuck dislocations move away in the opposite glide directions.

In each swell-shrink cycle, we determine the maximum number of dislocations in the crystallite (See Section 3.3.2). Thresholds are cusps in the dislocation number *vs.* a_{max} curve shown in Figure 3.4. We identify the first threshold diameter a_{T} when dislocations appear. Adding more particles to a side of the cluster s decreases the per-particle diameter threshold because less per-particle swelling is required to emit dislocations when the cluster is larger. By plotting the diameter thresholds for dislocations, we find that the diameter threshold scales linearly with $1/s$. To collapse the behavior across multiple cluster shapes by cluster side number s (an integer), suppose that at some length threshold ξ and change in length of a cluster side Δl, a dislocation is formed. However, as we saw from the infinite cluster corners, there is some amount of swelling below which any sized cluster will not create dislocations. Let Δa_∞ represent a diameter change that will not produce dislocations even for an infinitely large cluster. We represent this as:

$$\Delta l = l_{\mathrm{T}} - l_{\mathrm{init}} - l_\infty = s(a_{\mathrm{T}} - a_{\mathrm{init}} - \Delta a_\infty) \equiv \xi \tag{3.1}$$

We linearize equation 3.1 as follows

$$a_{\mathrm{T}} - a_{\mathrm{init}} = \xi \frac{1}{s} + \Delta a_{\infty} \tag{3.2}$$

where ξ is the slope of the line when plotting $a_{\mathrm{T}} - a_{\mathrm{init}}$ *vs.* $1/s$ and Δa_{∞} is the y-intercept. Figure 3.5 shows the threshold data plotted in the form of Equation 3.2 to determine Δa_{∞}. As $s \to \infty$, $a_T \to a_{init} + \Delta a_{\infty}$. When swelling a cluster of any size to $a_{max} = a_{init} + \Delta a_{\infty}$, it will not emit dislocations.

Our finding of $\Delta a_{\infty} \approx 0.07$ is commensurate with the diameter thresholds of particles in corners embedded in the crystallite, which begin producing dislocations at $a_{max} \approx 1.09$ per Table 3.1, implying that these approximations of infinite clusters had $\Delta a_{\infty} = 0.09$. We see the data collapse when plotted as a log-log plot once we subtract off this Δa_{∞} in Figure 3.6.

The existence of a side-length threshold for dislocation emission suggests a way to control where dislocations emit. To have repeatable dislocation motion, choose a_{max} above the threshold.

3.4.2 Manipulating cluster side length to bias dislocation emission

As we showed in the previous section, unlike cluster shapes with all acute or all obtuse corners that tend to form dislocation pairs on all corners simultaneously, the parallelogram cluster first forms dislocation pairs at its acute angle corners. When a dislocation pair appears at a corner, the emitting dislocation can move along one of two glide planes bounding that corner of the cluster. Due to the sensitivity of dislocation emission to the threshold, we hypothesized that we can use asymmetric side lengths to selectively emit dislocations on one glide plane. We relax some of the initial constraints around cluster shapes to control where the corner sends dislocations. First, we try asymmetric parallelograms. Then, we relax the need to have straight, smooth edges of the cluster. These actions amount to ways of shortening one side of the cluster.

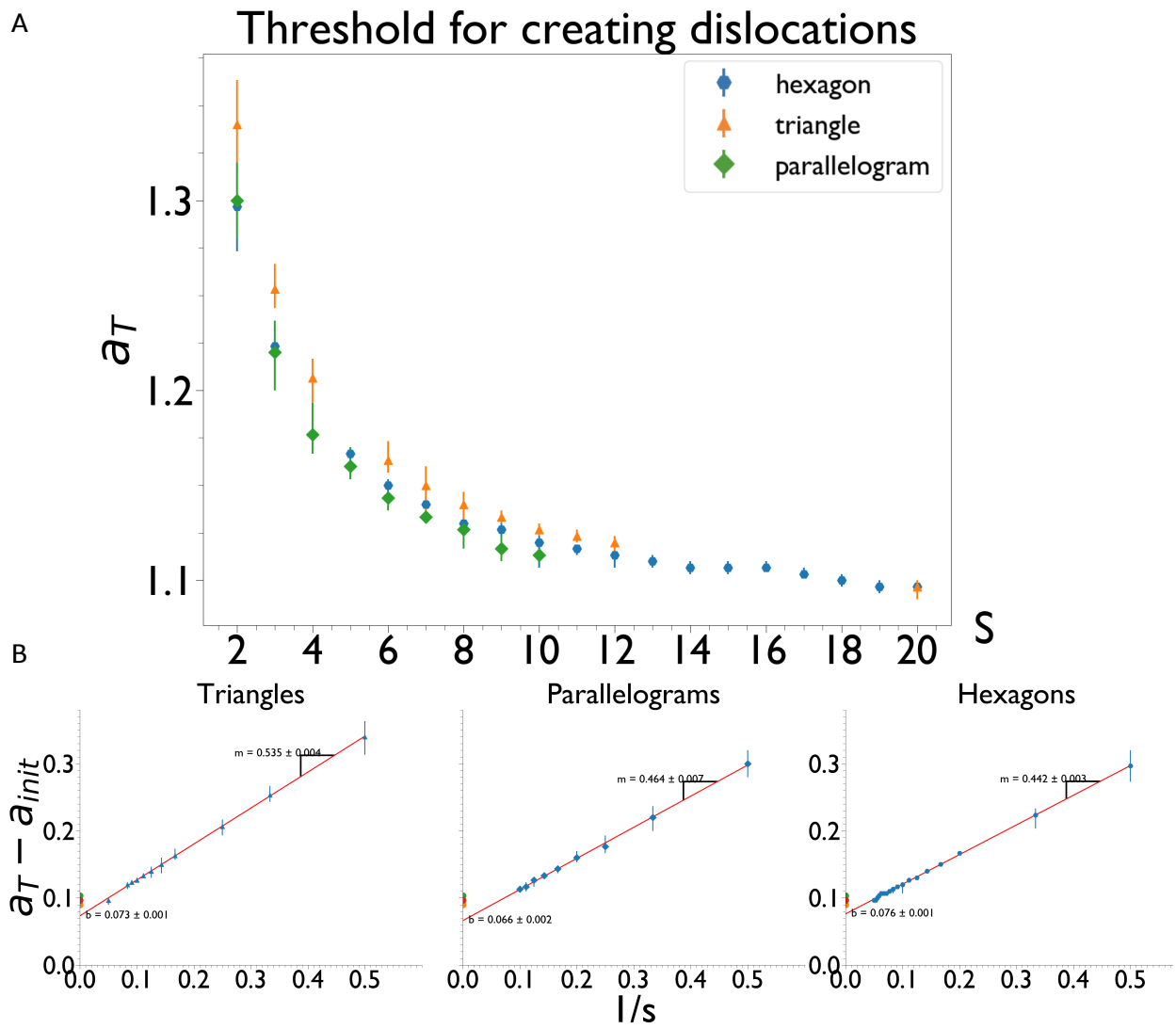


Figure 3.5. Thresholds for dislocation emission. (A) Diameter threshold a_T vs. particles in a side s. (B) Linearized diameter threshold curves for emission of dislocations in triangle, parallelogram, and hexagon clusters of side length 2–20 to determine Δa_∞ from Equation 3.2. The best fit lines are plotted. Filled circles show "infinite" cluster shapes that are different angled corners extending to the boundary of the crystallite from Table 3.1.

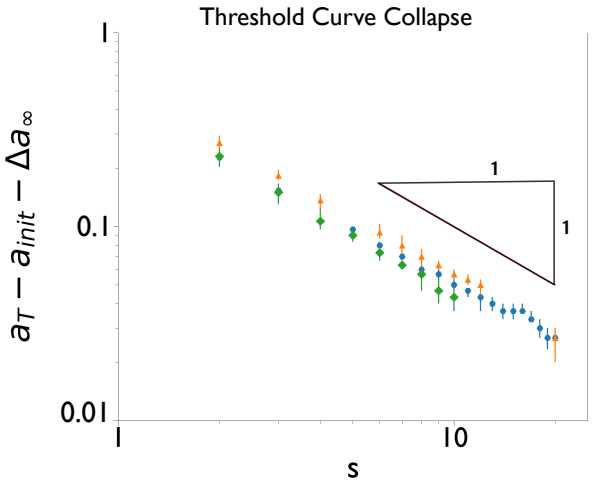


Figure 3.6. Linearized dislocation threshold curve.

We run 5 swell-shrink cycles for 9×10 through 4×10 parallelograms and count how many dislocations emit along each glide plane and the direction of emission. Figure 3.7A shows the dislocation paths around these clusters, showing how the more asymmetric the parallelogram, the more dislocations emit along the $120°$ and $300°$ glide planes. Fig 3.7B plots the number of dislocations that emit along each glide direction, normalized by the total number of dislocations emitted from that cluster shape, showing the biasing effect. Applying the threshold analysis of equation 3.2, the threshold diameters are $a_T(s = 10) = 1.05$ and $a_T(s = 4) = 1.25$. Swelling to $a_{max} = 1.16$ of the 4×10 parallelogram puts only the long side above the threshold, effectively biasing dislocations to emit along the glide plane bounding that side.

Another way to reduce the effectiveness of a certain edge of the cluster emitting dislocations is to remove some particles (*e.g.*, every other one) from a side. If a side of a cluster is perforated in this manner, that side can be brought below the threshold for creating dislocations, and that side will show reduced dislocation emission. In Figure 3.8B, we show how we can invert the effect from above, where by perforating the $s = 10$ side of a 9×10 parallelogram cluster, we cause the shorter $s = 9$ side to emit dislocations. Thus, a regular parallelogram with two perforated sides can behave like an asymmetric parallelogram.

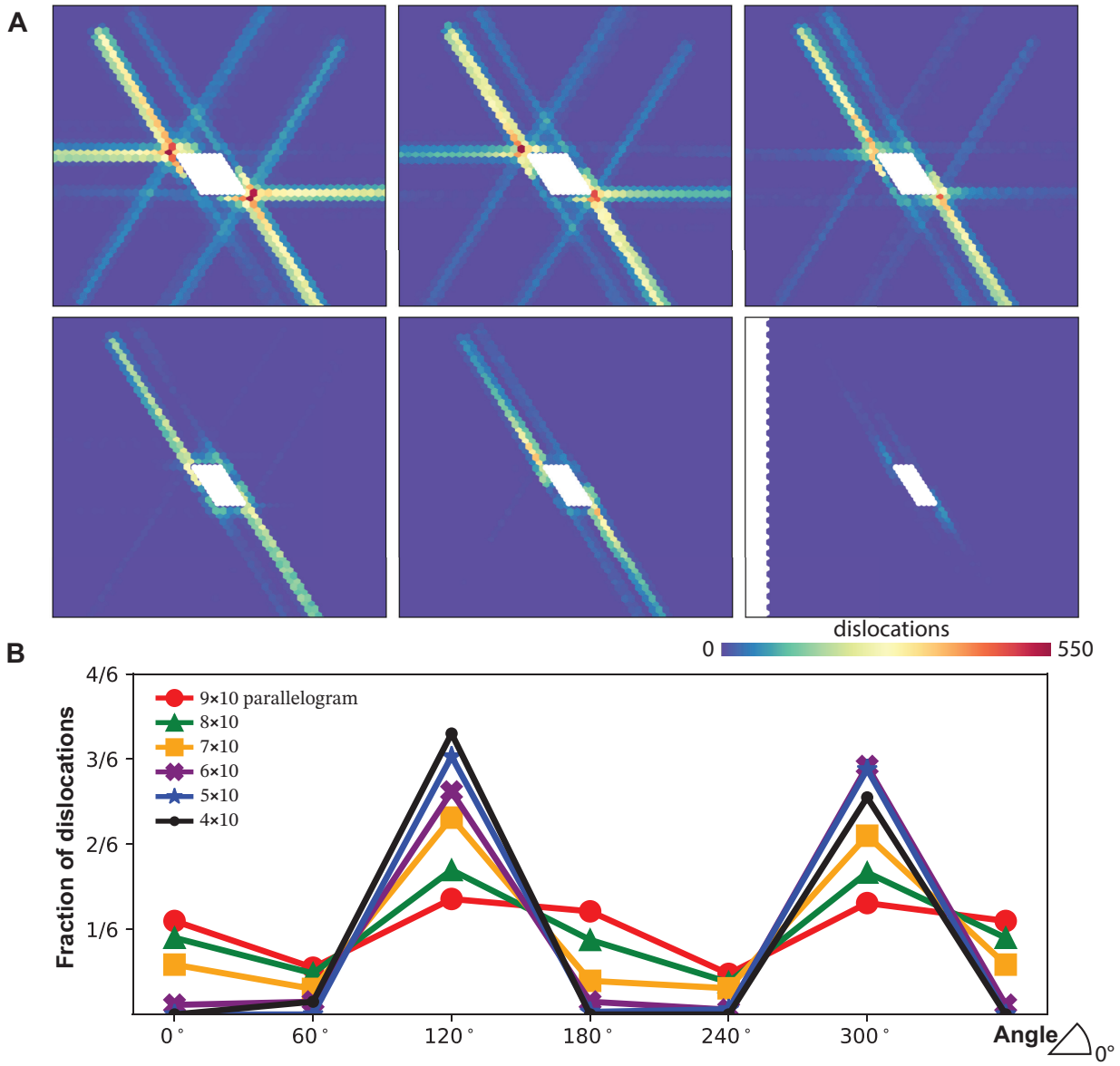


Figure 3.7. Side length biases dislocation direction. The parallelogram cluster is active on the acute corner, which provides a place to bias the directions that dislocations are emitted. **(A)** Heat maps showing common dislocation paths around parallelogram clusters, from 100 replicate simulations of 5 swell-shrink cycles each. Color bar represents the count of times a dislocation passed near a particle. **(B)** The glide directions of dislocations emitted from size $n \times 10$ clusters ($n \in \{4, 5, 6, 7, 8, 9\}$). The $360°$=$0°$ data is shown for ease of reading. The total number of dislocations for each cluster shape is: {4:40, 5:398, 6:321, 7:820, 8:1206, 9:1486}. This figure was created in collaboration with Nipuli Gunaratne, an undergraduate student I mentored.

We arrive at the following design rules.

1. Position target glide planes at acute angle ($60°$) corners of the cluster shape.

2. Swell the cluster particles above the threshold diameter.

3. Deactivate unwanted glide planes with shorter or perforated sides.

Using the design rules, we can predict the dislocation emission patterns around more complex cluster shapes. Figure 3.8 shows the heat maps around trapezoids, doubly-truncated triangles, and rough-edged parallelograms as well as the deformation of the crystallite resulting from repeated swell-shrink cycles. A trapezoid can be seen as an equilateral triangle with a truncated corner with long side length s and short parallel side length s_{top} making diagonal side $s_{diag} = s - s_{top} + 1$. When the maximum swollen diameter activates the acute angle corners, only the longest side will emit dislocations. The effect is enhanced because the truncation replaces the $60°$ corner with two $120°$ corners, which have an even higher dislocation nucleation threshold. When we swell the trapezoid to a_{max} of 1.16, we observe dislocations emitting parallel to the longest side. Figure 3.8A shows the effect that the dislocations emitted by the two active acute corners have on the crystallite. Since corner truncation is a way to select on which glide planes dislocations form, we next truncate two corners of a triangle.

Truncating two corners of the triangle results in a "hexagon hat", leaving the one $60°$ corner to emit dislocations. As shown in Figure 3.8C, we observe the acute corner bounded by the longest sides to be the most active emitter of dislocations. The sides bounded by obtuse angles have side length s_{hex} and the side adjacent to the acute angle have side length $s_{point} = 2s_{hex} - 1$. The triangle that the hexagon hat started from would have side length $3s_{hex} - 2$. For this cluster, we chose a_{max} to be between that of a hexagon with side length s_{hex} and triangle with side length s_{point} to activate the acute corner bounded by long sides without activating the obtuse corners bounded by shorter sides. Figure 3.8D applies

perforation to deactivate one side of the "hexagon hat" cluster, causing the dislocations to emit from the flat side of the active acute angle corner.

3.4.3 Concave Clusters

Finally, we examine concave clusters formed by removing a wedge of particles from a hexagon cluster. Figure 3.9 shows the most likely dislocation paths around a hexagon with $60°$ and $120°$ wedges of particles removed. The concave parts of the shape don't emit dislocations because there is no place for both dislocations in the pair to emit along the glide plane. The dislocation pair needs to access the entire glide plane for both to emit.

3.5 Discussion

Our work provides more insight into the performance of the "double half ellipse" cluster investigated in previous work [43]. The purpose of the "double half ellipse" is effectively to create an acute angle. Previous work also disrupted the side of a cluster to bias dislocation emission, but by removing a group of 5 particles near one corner called a "notch". The notch relieved strain around the nearby corner, therefore deactivating it. If we could deactivate the third side of our parallelogram cluster, we could match its performance with a simpler shape that may be easier to fabricate in an experimental system.

In an experiment involving careful positioning of particles, we need to know how many swellable particles are needed to affect the system. The quantitative results from Figure 3.5 form a heuristic to screen experimental systems based on how much the particles can swell and how many can be patterned into a cluster. We suspect that the ability to construct straight sides in the experimental cluster will be the limiting factor in a potential experiment. Patterning particles into a cluster could be done via template-assisted assembly [26] or projecting an optical pattern with a digital micromirror device [82, 83]. The material will limit the maximum particle diameter. There are various swellable polymers that are

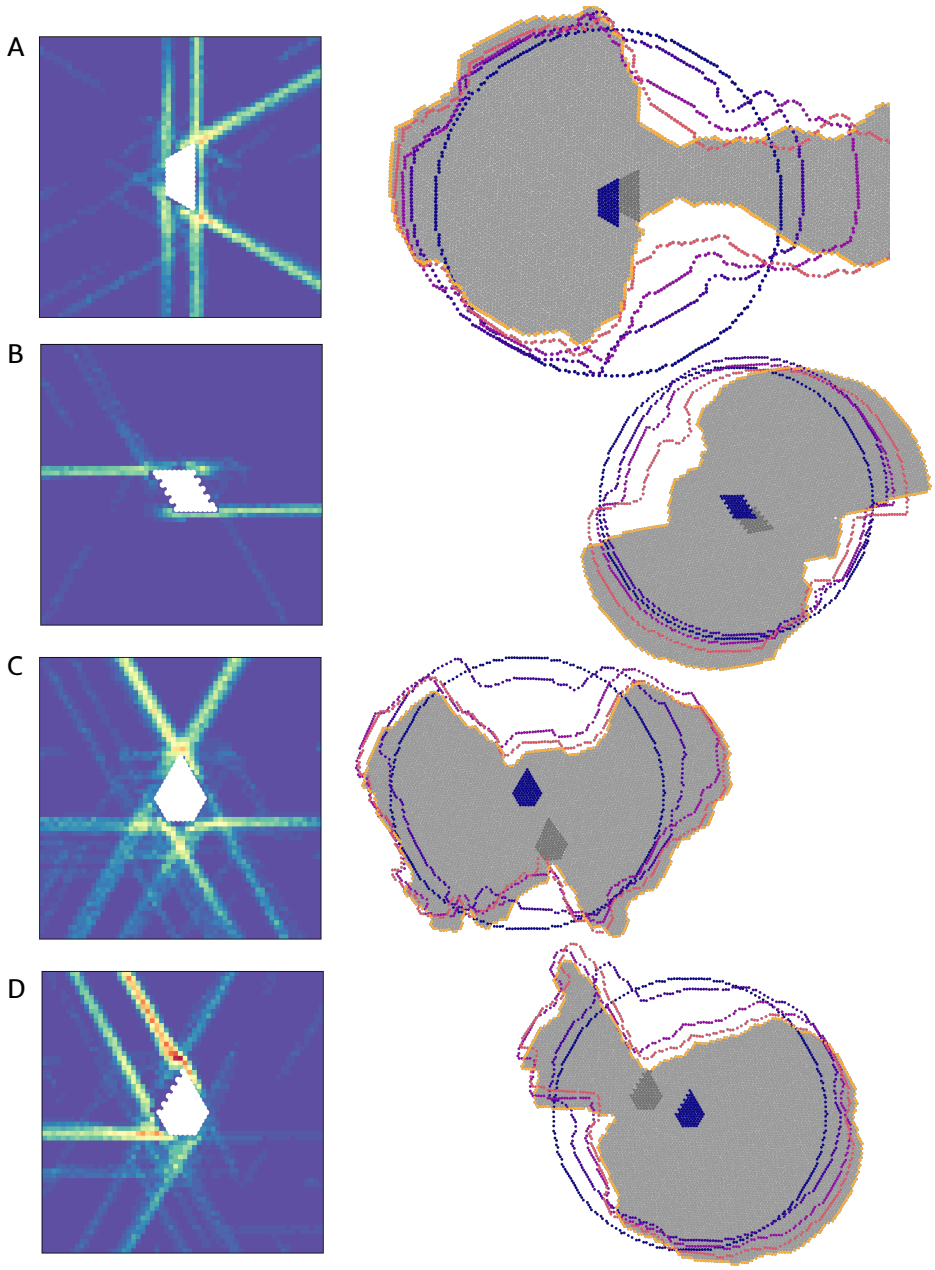


Figure 3.8. Application of swelling cluster design rules. Final simulation snapshots and intermediate crystallite outlines for simulations of 100 cycles for more complex cluster shapes to a_{max} of 1.16. The shapes are shown in the heat maps to the left. The colored points are particles along the outline of the crystallite on frames {0, 400, 1200, 2200, 3200} and the gray particles are the positions on frame 3200. The initial/final locations of the cluster particles are colored blue/dark gray. **(A)** A trapezoid cluster, which can be thought of as truncating one corner of a triangle, exhibits greater activity along the longer side that is bounded by acute corners. **(B)** Here, we turn off one set of parallel sides of a symmetric parallelogram by removing particles from one side. Those sides behave like smaller sides that are below the threshold. **(C)** The hexagon hat cluster is active on the acute angle bounded by the longest sides. **(D)** Roughening one of the longer sides of the hexagon hat cluster biases the dislocations to emit along the glide plane defined by the smooth side.

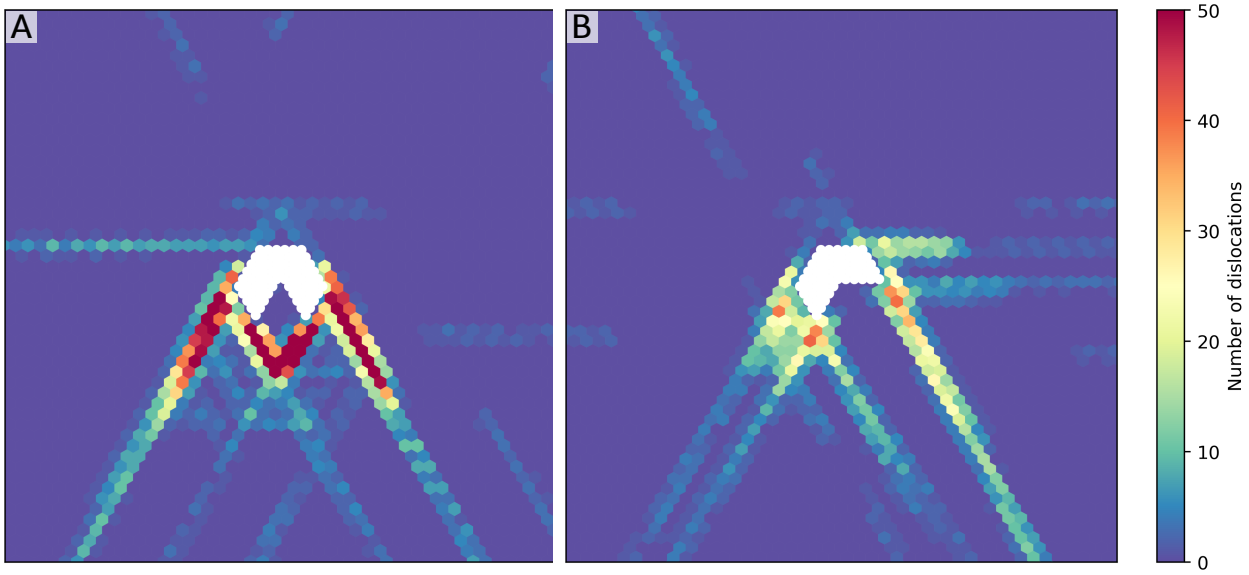


Figure 3.9. Dislocation paths for hexagon with wedge cutouts. (A) Acute angle (60°) cutout. (B) Obtuse angle (120°) cutout. Formed from 10 replicas of 5 cycles each, swelling to $a_{max} = 1.18$.

promising [84]. Liquid crystalline elastomer particles can be made in large numbers [36]. This material swells when crossing the nematic-isotropic transition of the liquid crystal, whether that is caused by a change in temperature, concentration, or magnetic field [85]. Another polymer of interest is PNIPAm, which swells when heated [35]. We performed simulations of particles interacting with the Mie potential and observed the same trends, suggesting that the mechanism is robust to different swellable particle systems. Defects are hard to fully eliminate in experimental systems. The presence of defects in the crystal would slow down or redirect some of the dislocations, but with enough swell-shrink cycles, the desired dislocations should surpass the defects in the way, and the effect of the designed cluster geometry would persist.

This chapter examined single swellable clusters. Including multiple clusters increases the design space of possible dislocation interactions and therefore of crystallite morphological changes. Our design rules based on corners and side lengths serve as a guide to controlling dislocation motion, toward designing colloidal robotic actuation.

CHAPTER 4

Dislocation Logic: Shear Activated Logic Operations in Colloidal Crystals

4.1 Abstract

The collective behavior of colloidal particles can be used to achieve certain robotic functionalities. In crystals, purposefully engineered dislocations created by the swelling and deswelling of an embedded cluster of swelling particles can change the shape of a colloidal crystallite in a programmable way. In this work, we show using simulations how dislocations in colloidal crystals can function as Boolean logic gates. The presence of a dislocation along prescribed input or output glide planes is defined as logical True. Logic gates consist of clusters of swelling particles in fixed positions, relative to the input and output glide planes. We generate dislocations with clusters of swelling particles for both input and internal dislocation sources. We demonstrate an AND gate with two internal swelling clusters. The NOT gate introduces a blocking cluster that prevents a dislocation from moving forward until it can be released by internal recombinations. We further feed the output of an AND gate to a NOT gate, with a delayed swelling operation, to produce the universal logic NAND gate. The results suggest the ability to bridge sensing, computation, and actuation in colloidal crystal systems.

4.2 Introduction

In a colloidal crystal, plastic deformation — the bulk rearrangement of particles via the motion of dislocations — can be seen as actuation. By controlling dislocation creation and migration with clusters of swelling particles embedded in a colloidal crystallite, we can control the shape of the crystallite.

In Chapter 3, we focused on creating dislocations by exploiting geometric features of the shape of the cluster of swelling particles, showing that the long sides of the shapes defined where dislocations tended to emit. However, some dislocations emit from the cluster along other glide planes. For example, for the parallelogram cluster, some dislocations emit on glide planes not parallel to any side. These are caused by dislocation reactions between dislocations that form on adjacent sides. This project aims to harness the interactions of multiple dislocations and multiple clusters to achieve simple computations.

Dislocation motion can be seen as transmission of information, not just the transmission of shear deformation, inspired by various physical computing systems [57, 55, 54, 60]. If we see dislocation motion as information transfer, then dislocation reactions are a form of information processing. If we can form a mapping between the motion and interaction of dislocations to Boolean logic, then we can say that dislocation recombination is equivalent to dislocation "computation."

Previous computational work has used disclinations, a type of defect in liquid crystals, to encode logic operations in those systems [67, 68]. In nematic liquid crystals, disclinations occur at discontinuities in the director field. A key active nematic system is formed of cell microtubules and motor proteins [65]. By using a modified myosin protein instead of kinesin, the activity can be made sensitive to light, and therefore able to be patterned optically [66].

Previous work has used disclinations as logic carriers for logic-like operations [67]. The system comprised the patterned active region and the shape of the system boundary. The driven $+1/2$ defect moves in the active region and can be confined there. The system does

not need external driving forces, but needs precise patterning of the light as well as fixing of the director field at the boundary (homeotropic anchoring). The authors showed how the passage of one defect stops the motion of another defect, which could be used like a transistor "gate". Notably, these were not Boolean logic gates.

A second simulation was done using a nematic liquid crystal on the surface of a sphere, this time achieving Boolean logic gates (as well as other forms of logic gates) [68]. Logical true was represented by a $+1/2$ defect. The input orientation was set with an external field that interacts with the nematic crystal. Inputs and outputs were controlled and measured at different positions along the surface of the sphere, meaning that it was not possible to take the output from one gate and feed it to another gate.

The benefit of using dislocations as signals is the connection to deformation in crystals. The signal is the actuation. This circumvents the need to transduce a sensed signal to an electrical signal to do traditional computation, and then convert the results back to physical sensation with an actuator. The colloidal crystallite presents a unique medium in which to combine robotic functionalities of dislocation computation and actuation.

In experiments, dislocations can be created by shearing [48] or by rotating [49] a colloidal crystal with optical tweezers. Once created, a dislocation moves in response to the local shear on its glide plane. Cyclical shearing [86] or external oscillating electric fields [87] can remove defects in a colloidal crystal. Clusters of swelling particles within a colloidal crystallite will emit dislocations [43]. Shearing the crystal provides a driving force to move dislocations.

In this chapter, we design and demonstrate simple Boolean logic gates that operate using dislocations as their signals, with a $(1, 0)$ dislocation defined to be logical True. Each logic gate is designed around fixed input(s) and output glide planes. Internal clusters of swelling particles in fixed positions produce dislocations to react with the input dislocation(s) to produce the desired outputs. The AND gate can be fed into a NOT gate, producing the NAND gate, from which all other gates can be derived, providing a complete set of logic

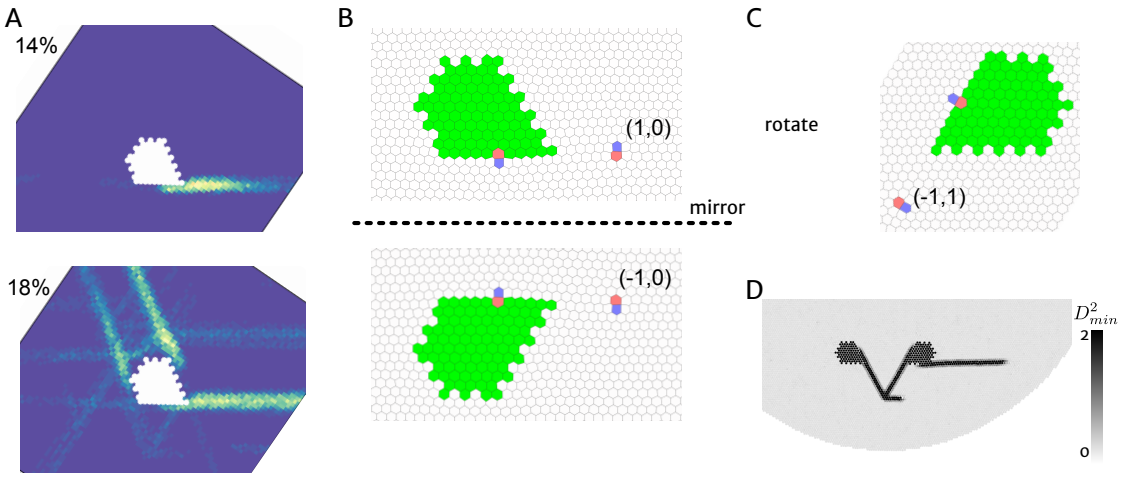


Figure 4.1. Design of a cluster emitting one dislocation pair. (A) Heat maps showing the performance of the logic cluster. We operate in a swelling regime where only the acute angle is active in emitting dislocations. (B-C) Voronoi decomposition of the particles around the swelling cluster as it emits a dislocation pair. Mirroring (B) and rotating (C) the cluster emits dislocations with any needed Burgers vector. (D) The paths of dislocations emitted from two clusters, shown via minimum non-affine squared displacement. The dislocations recombine and begin gliding in the horizontal direction.

operations for general computation within the crystallite. The ability to embed logic into colloidal crystals via defects could open opportunities to design their optical or physical responses bridging sensing, computation, and actuation.

4.3 Results

We build on our work in Chapter 3 in designing clusters to emit a pair of dislocations. We simulate a 2D crystallite with two particle types: swellable particles positioned in multiple clusters, and passive particles elsewhere. First, using the design rules from Chapter 3 we design a cluster that reliably generates a dislocation pair. The design, shown in Figure 4.1A, consists of a triangle merged with a hexagon with 4 of 5 of the sides perforated (missing particles). The swellable particles in clusters are harmonically bonded to their neighbors. When the particles in the cluster swell (we swell by 14%), a dislocation pair is created, and a $(1,0)$ dislocation emits to the right. We take as our basis the non-orthogonal basis vectors $\vec{r} = \hat{x}$ and $\vec{s} = \frac{1}{2}\hat{x} + \frac{\sqrt{3}}{2}\hat{y}$ and write Burgers vectors as (r,s). A $(-1,0)$ dislocation can be

emitted by mirroring the cluster, as shown in 4.1B. The other needed dislocations can be formed by rotating the cluster, for example as shown in 4.1C.

Before designing gates, we design a simple recombination of dislocations from two swelling clusters. Dislocations generated by two swelling clusters can be guided to react with each other. Figure 4.1D shows the path of such dislocations by coloring particles with their per-particle minimum non-affine squared displacement, D^2_{min} (see Section 2.2.3). Here, a $(-1, 1)$ dislocation from the cluster on the left glides diagonally down and to the right to meet a $(0, -1)$ dislocation from the cluster on the right. They recombine to form a $(-1, 0)$ dislocation.

This example already serves as a basic mechanism of an AND gate. If both clusters swell, the reacted dislocation glides along the x direction. If only one cluster swells, the dislocation glides towards the boundary at the lower part of the crystallite. However, the inputs and outputs are along different glide planes, which would make it challenging to sequence multiple gates together. Therefore, we need to design constraints to achieve Boolean logic gates.

4.3.1 Dislocation Logic Scheme

We impose the constraint that our dislocation logic gates take inputs from the left and emit output to the right. The dislocations that glide in the horizontal direction have Burgers vector $(1, 0)$ or $(-1, 0)$. In our scheme, the presence of a dislocation of Burgers vector $(1, 0)$ along a designated input or output glide plane(s) is considered "True".

We apply a global shear force F_{shear} to all particles in the system to drive dislocations so that the $(1, 0)$ dislocation is swept to the right. Shear is a common way of interacting with colloidal crystals [49, 88]. We use $\vec{F}_{shear} = (my, 0)$ with $m = 1 \times 10^{-4}$ for the AND and NOT gate simulations, and $m = 5 \times 10^{-5}$. The longer simulations use a smaller shear to avoid the shear itself from deforming the crystallite.

Designing a gate requires specifying:

1. The input glide planes to receive dislocations.

2. The output glide plane that the output will appear on.

3. The positions of the internal swelling clusters.

The input(s) to the gate are fed along designated input glide planes on the left, and the output is along the output glide plane on the right. Each gate consists of internal dislocation-generating clusters of swelling particles. These internal clusters remain for each set of inputs. The internal clusters have different orientations to emit different dislocations as designed. The internal clusters produce $(-1, 1)$, $(0, -1)$, or $(1, -1)$ dislocations (as well as their opposites). The other half of each dislocation pair sticks to the cluster upon swelling, and emits during the shrinking phase.

The logic gates are fed with input dislocations. These could be outputs from prior dislocation logic gates, dislocations already in the crystal, or dislocations created with optical tweezers [47]. The input(s) and outputs are always dislocations.

For our demonstrations, we trigger each logic gate with dislocations generated by swellable input clusters. The input clusters are not considered part of the gate. Input clusters could be responsible for sensing environmental changes that induce swelling or are the controlled input on the lab bench. To implement sensing, each input cluster should be responsive to a different environmental stimulus. This could be prototyped in experiment with projected light patterns from a digital micromirror device [37, 82, 83]. An input cluster only swells if that input is set to "True". Otherwise, the cluster is inactive. The input clusters always produce a dislocation pair consisting of $(1, 0)$ and $(-1, 0)$ dislocations, where we use the $(1, 0)$ dislocation as the input.

The timing of the dislocations affects the signaling and operation of the logic gates. The speed of a dislocation is proportional to the force on its glide plane, which is proportional to the shear force in the direction of the glide plane. The distances between logic gates are set so that the dislocations arrive at the correct time to recombine in the designed reactions.

In our demonstrations, particles in the input clusters and internal clusters swell and shrink with the same swelling cycle.

During the operation of each gate, other dislocations form and react, but the output always ends up as the presence or absence of a $(1, 0)$ dislocation on the output glide plane. The output dislocation is free to enter another logic gate or propagate to the surface of the crystallite to deform it. Below, we first design and test an AND gate and a NOT gate, then combine them to form a NAND gate and demonstrate the feasibility of sequencing gates together.

4.3.2 AND Gate

The AND gate reads dislocations on two input glide planes from the left and outputs a dislocation to the right if both input dislocations are present. Therefore, it takes a total of $\sum b_{in} = (2, 0)$ and outputs $(1, 0)$. Internally we must provide $(-1, 0)$ of dislocation to react with it. Since there are two inputs, we split this into two internal dislocations and use internal dislocations $(-1, 0) = (-1, 1)^{top} + (0, -1)^{bottom}$. Thus, the AND gate has two internal clusters to generate these dislocations.

Input dislocations enter on parallel glide planes, and the output dislocation is on a glide plane halfway between them. The internal clusters produce diagonal dislocations, which react with input dislocations. Figure 4.2 shows the design and truth table for the operation of the AND gate.

For AND(True, True), first the inputs react as so:

$$(1, 0) + (-1, 1) \rightarrow (0, 1)$$

$$(1, 0) + (0, -1) \rightarrow (1, -1)$$

The resulting $(0, 1)$ and $(1, -1)$ dislocations then glide to the center and react to create the output $(1, 0)$ dislocation on a glide plane midway between the input glide planes. If

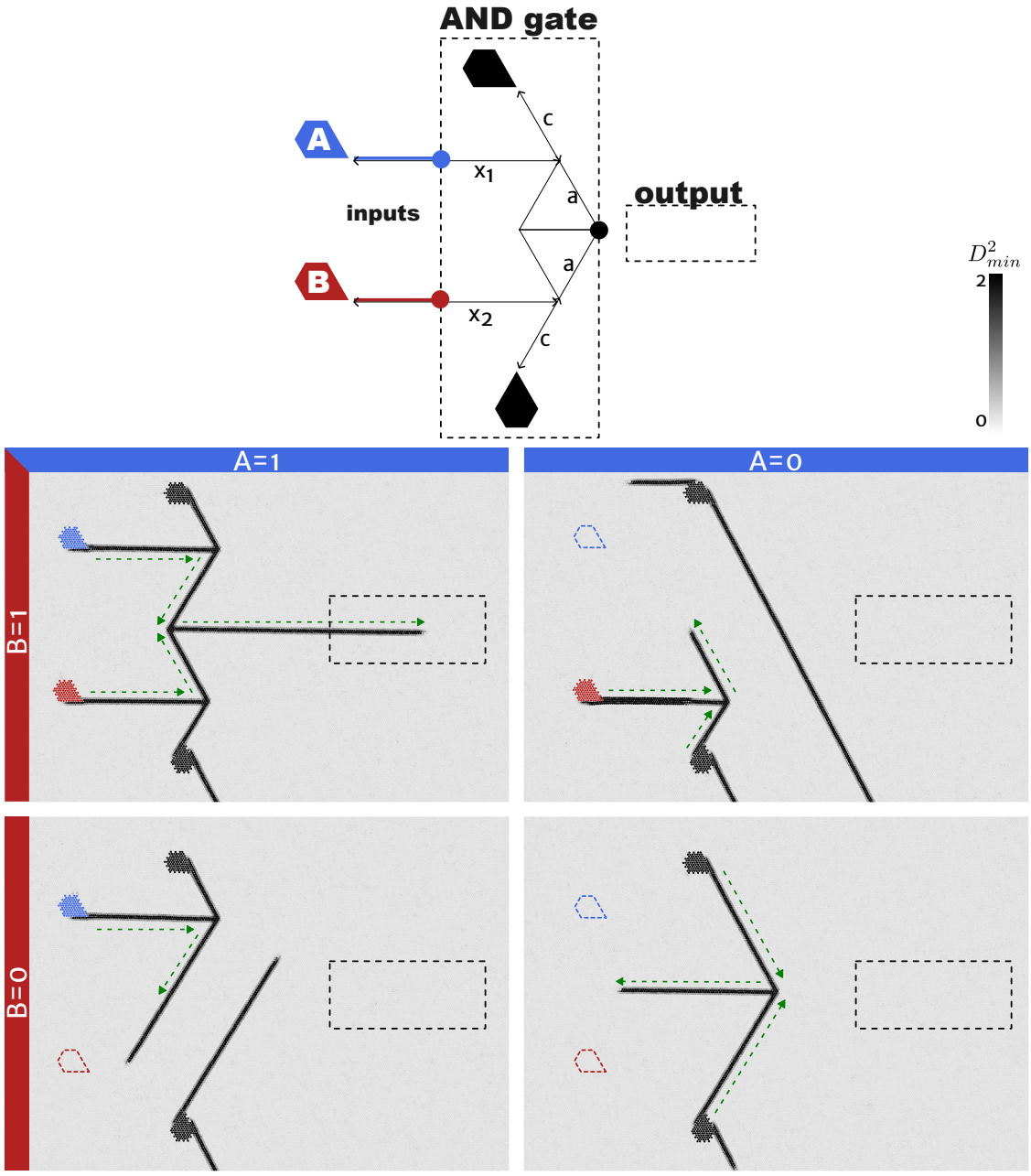


Figure 4.2. Design and operation of the AND gate. (below) Truth table, showing input clusters in blue and red. Particles are colored by their minimum non-affine squared displacement D^2_{min}, showing passage of dislocations, with motion annotated in green dashed lines. The output zone is indicated with a dashed rectangle. For AND(True, True), each input dislocation reacts with its respective internal dislocation, then again to yield a dislocation on the target output glide plane. For one True input, dislocations exit the gate in diagonal directions. For AND(False, False), a dislocation exits to the left. Inactive swelling clusters are indicated by a dashed outline.

either of the input dislocations is not present, no dislocation passes the output zone. An extraneous dislocation leaves at a diagonal direction. In the AND(False, False) case, the internal clusters produce a $(-1, 0)$ dislocation that exits the left side of the gate.

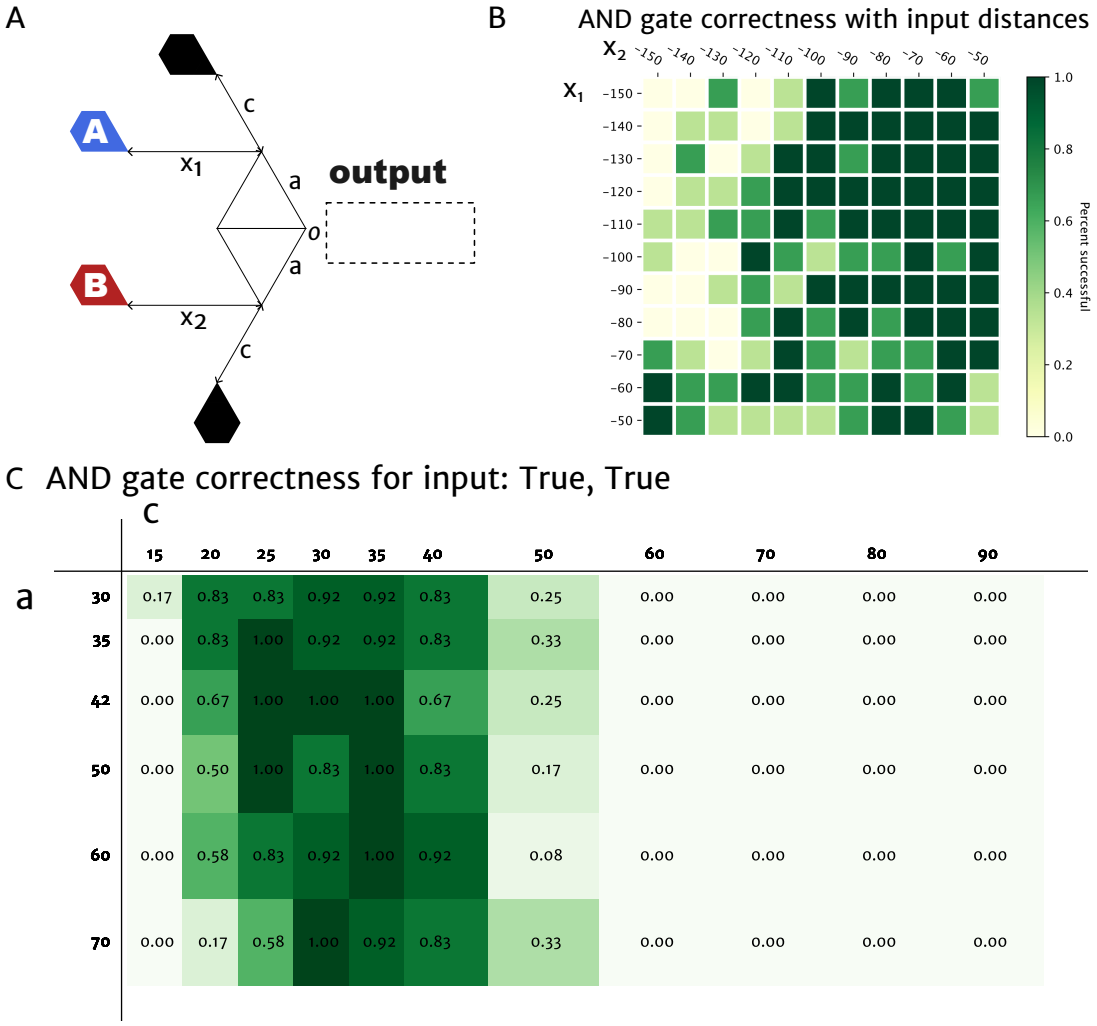
Figure 4.2 shows the design parameters of the AND gate. The designed reactions occur at the points of a triangle with side length a. The second design parameter is the distance from the reacting points to the internal clusters c.

4.3.3 Correctness of the AND Gates

We quantify the performance of the gate by tracking dislocations on every simulation frame. A gate is defined to be correct if the presence (or absence) of a dislocation on the output glide plane corresponds with the result of the logic operation. For example, if our gate produces AND(True,False) = False (no dislocation on the output glide plane), it is correct for that replica. The correctness for a particular combination of design dimensions is the fraction of replicas that were correct. We look for the presence of a dislocation in the output zone to make sure it corresponds to the result of the output of the logic gate. With the origin at the corner of one of the triangles as shown in Figure 4.3, for the AND gate, the output zone is for x between 10 and 60 particle diameters to the right of the origin and for y between -8 and 8 particle diameters above and below.

The AND gate is said to be correct if a dislocation appears on the output glide plane, which is to the right of the origin. As shown in Figure 4.3C, the performance of the gate in insensitive to the value of a over a wide range studied. However, c must be small enough that internal dislocations can react with the input dislocations.

The performance of the gate is sensitive to the distance between the reaction points and the input clusters; however, this is an application consideration and not central to the gate design itself. Figure 4.3B shows the performance of the gate as a function of the distances from the input cluster to the internal reacting point of the gate. We find that the result is not symmetric with respect to input cluster distances because the input clusters can interfere



a \ c	15	20	25	30	35	40	50	60	70	80	90
30	0.17	0.83	0.83	0.92	0.92	0.83	0.25	0.00	0.00	0.00	0.00
35	0.00	0.83	1.00	0.92	0.92	0.83	0.33	0.00	0.00	0.00	0.00
42	0.00	0.67	1.00	1.00	1.00	0.67	0.25	0.00	0.00	0.00	0.00
50	0.00	0.50	1.00	0.83	1.00	0.83	0.17	0.00	0.00	0.00	0.00
60	0.00	0.58	0.83	0.92	1.00	0.92	0.08	0.00	0.00	0.00	0.00
70	0.00	0.17	0.58	1.00	0.92	0.83	0.33	0.00	0.00	0.00	0.00

Figure 4.3. Correctness of the AND gate. (A) The design dimensions of the gate. The size of the reacting triangle a sets the vertical distance between the input glide planes. The internal clusters are spaced a distance c away from the reaction point. Parameters are expressed in terms of lattice distances. (B) The correctness of the AND gate with respect to different spacing of the input clusters, 3 replicas per combination. (C) The correctness of the AND gate in changing internal dimensions a and c over 2 values each for x_1 and x_2, fixed swelling parameters, and 3 replicate simulations. Result of 6 simulations averaged.

if they are too close. Further, we note that the diagonal of x_i is less preferred. Parallel dislocations separated only in the y direction have regions of stability offset from each other [45] along an angle, so the staggered input configuration provides a more reliable gate.

Based on the results in Figure 4.3C, we choose parameters for the AND gate of a: 40, c: 30.

4.3.4 NOT Gate

The NOT gate has the apparent challenge of creating a dislocation out of nothing. That is, the input of a $(1, 0)$ dislocation should not output a dislocation; the input of no dislocation should output a $(1, 0)$ dislocation. Therefore, the gate must internally catch the input dislocation or generate the output dislocation.

Importantly, dislocations react according to the Frank criterion, which states that for dislocations to react, the sum of squared magnitudes of their Burgers vectors must decrease [45]. We use the Frank criterion to "catch" the input dislocation for NOT(True).

We introduce the idea of using an internal cluster of bonded, but not swelling, particles to prevent passage of a dislocation. The bonded particles do not reconfigure, which prevents the topological defect from passing through. This would be a way to take the $(1, 0)$ input and prevent output, but we also need to release a dislocation if no input is present. For this, we internally create a $(1, 0)$ dislocation that is blocked by the internal cluster. We set up two reactions to direct the dislocation around the blockage. We create $(0, 0) = (-1, 1)^{top} + (1, -1)^{bottom}$ dislocations. The left inner cluster produces a $(1, 0)$ dislocation that glides to the right and is blocked. The top cluster produces a $(-1, 1)$ dislocation, and the bottom cluster produces a $(1, -1)$ dislocation. These internal clusters set up reactions to get around the obstacle, as shown in Figure 4.4. The output zone is below and to the right of the blocked cluster.

When computing NOT(False), the top $(-1, 1)$ dislocation reacts producing $(-1, 1)$ +

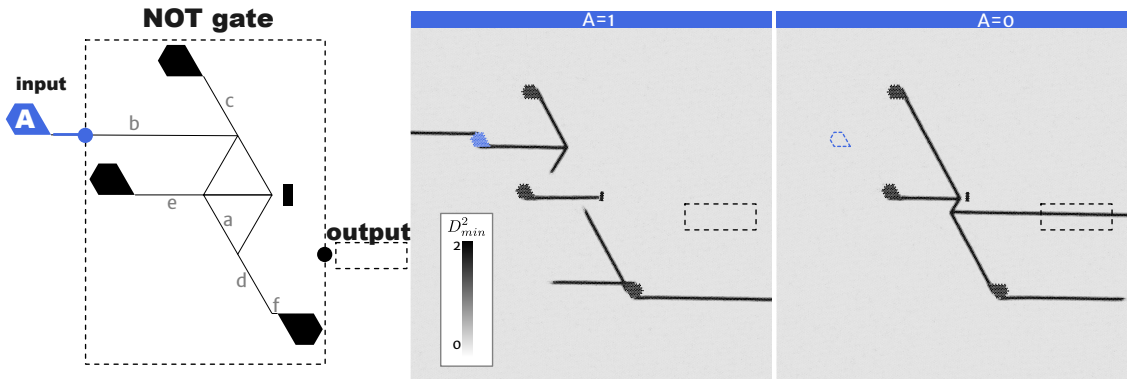


Figure 4.4. Design and operation of the NOT gate. The parameters are a: 42, b: 55, c: 40, d: 30, e: 0, f: 32. The core reacting zone is a triangle with length a. The top and middle internal clusters are distances c, e from their respective reaction points. The lower cluster is a distance d away and additionally a distance f to the right. (right) Designed dislocation reactions of the NOT gate. Computing NOT(False), the dislocations combine to get around the obstacle and emit True. Computing NOT(True), the resulting dislocation configuration is highly unlikely to react. Particles are colored by their minimum non-affine squared displacement D^2_{min}. Inactive swelling clusters are indicated by a dashed outline.

$(1, 0) \rightarrow (0, 1)$, which then reacts with the bottom $(1, -1)$ dislocation to produce the $(1, 0)$ dislocation of the output.

When computing NOT(True), the input $(1, 0)$ dislocation intercepts the top $(-1, 1)$ dislocation, producing $(0, 1)$. The resulting configuration of $(0, 1)$ along with the dislocations $(1, 0)$ from the left and $(1, -1)$ from the bottom is highly unfavorable to react because the sum of their Burgers vectors is $(2, 0)$, violating the Frank criterion. Thus no dislocation is emitted from the gate.

The NOT gate has dimension parameters a, b, c, d, e, f, as shown in Figure 4.4A.

4.3.5 Correctness of the NOT gate

To check the correctness of the NOT gate, we check that the presence of a dislocation in the output zone corresponds to the value of the gate, and that the input dislocation successfully reacts for NOT(True). For the NOT gate, the output zone for x is between 50 and 150 and y between -30 and -5. Additionally, for the NOT gate, we ensure that the input dislocation reacts with the upper internal dislocation by checking that no dislocation appears with x

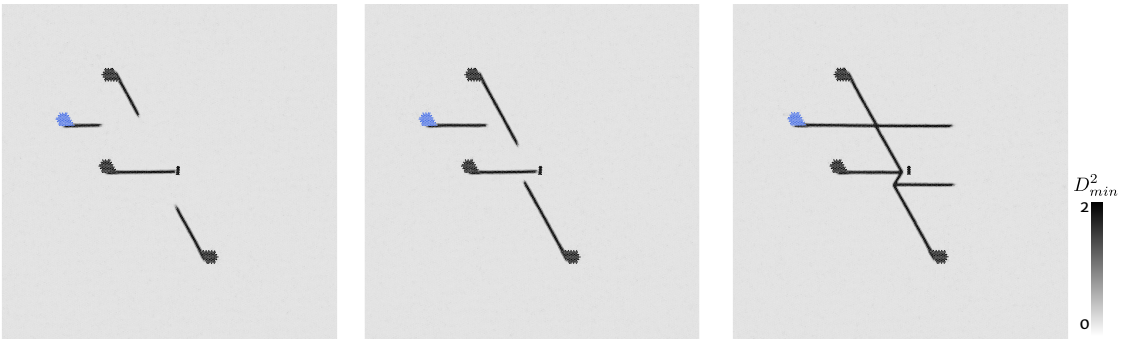


Figure 4.5. Example failure of the NOT gate. Simulation snapshots showing a common failure mode for the NOT gate computing NOT(True). The input dislocation does not intercept the top internal dislocation. Out of 10 trials, only one replica performed incorrectly. Parameters are a:42, b:55, c:40, d:30, e:0, f:32.

position 50 to 150 and y position within 3 units of the glide plane of the input cluster.

To find the NOT gate distance parameters, we first fixed a at 42 because that distance for the reacting triangle worked well for the AND gate. We ran a sweep of the Cartesian product of $b \in \{45, 55\}$, $c \in \{15, 20, 25, 30, 38, 40\}$, $d \in \{0, 10, 15, 20, 30\}$, $e \in \{0, 10, 15, 20, 30\}$, and $f \in \{22, 32\}$ with 3 replicates. For the configurations with over 90% correct, we ran 10 replicates. This set of replicates show that it can achieve 90% correctness.

10 of 10 replicates were correct for NOT(False), showing the ease of designing the redirection of dislocations. The correctness slips for the NOT(True) case. Figure 4.5 shows the most common failure mode where the internal dislocation fails to intercept the input dislocation. This is due to the randomness associated with the Brownian motion of the individual colloidal particles. If the random Brownian kicks happen to increase the local shear forces, a dislocation may reach the designed interaction area too early. 9 out of 10 replicas in this case succeeded.

4.3.6 NAND gate: Sequencing of gates

Finally, we show how the output of an AND gate can be fed to a NOT gate to create a NAND gate, which is a universal logic gate from which all other Boolean logic gates can be derived.

We introduce the idea of sequencing gates, wherein the swelling operation happens in succession, keeping pace with the position of the dislocation emitted for AND(True, True). The delay in swelling is analogous to a clock signal in traditional digital logic. One way to accomplish this in experiment would be to place the crystal on top of a substrate containing heaters to address heat to swell and shrink the clusters in the sequenced gates. Here, the swelling cycle of the NOT gate is delayed by one cycle relative to that of the AND gate.

Figure 4.6 shows the design and performance of the NAND gate. We position the NOT gate such that the output glide plane of the AND gate lines up with the input glide plane of the NOT gate. The dislocation appears in the output zone except when both inputs are True, demonstrating the NAND gate. Note that our NAND(True, True) results in a dislocation at a parallel glide plane above the output zone. We designed the NOT gate around an unfavorable reaction, and that reaction did not happen, but rather than the reactant dislocations getting stuck, a different reaction occurred. For this gate to operate for more than one cycle, the extraneous dislocation would need to be designed around.

4.3.7 Actuation of the Crystallite: Shear Activated Logic

Figure 4.7 shows how the AND gate can be used to conditionally deform a crystallite, so that a particular deformation only happens if both inputs are True. The darker colored particles have been rearranged by the passage of dislocations. The output dislocations of the AND gate emit to the right of the crystallite at a y-position midway between the input clusters and deform the surface of the crystallite. This change of the crystallite shape only occurs for AND(True, True). In the other cases, dislocations exit at other parts of the crystallite. The bottom figure of Figure 4.7 contains a truth table of only the input clusters operating within the crystallite with no gate clusters, serving as a control. By adding the two additional swelling clusters, we achieve this conditional deformation.

The driving force for this operation is the shear field. Without shearing the crystal, the input dislocations can't make it to the surface.

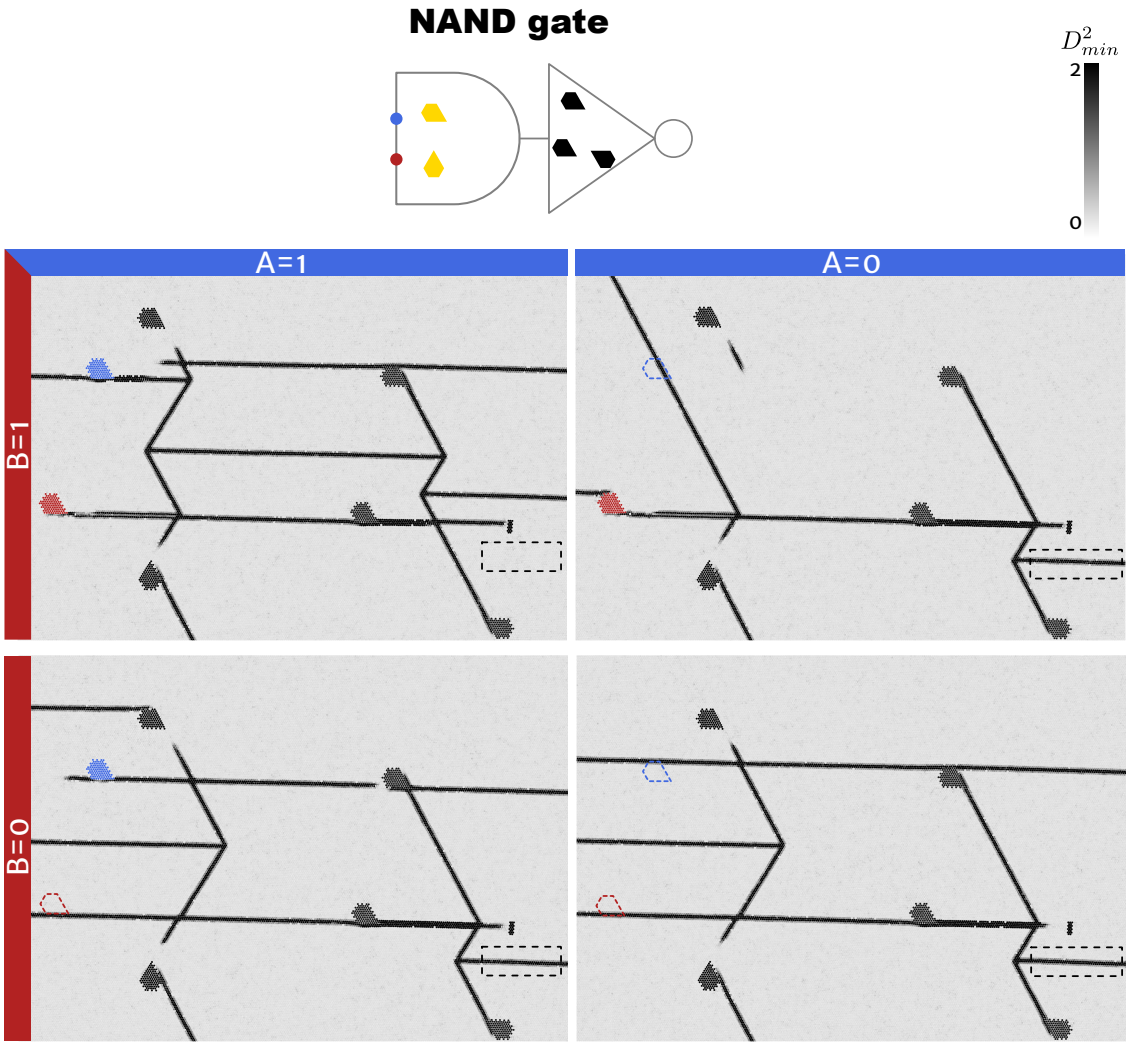


Figure 4.6. NAND gate from AND and NOT gates. (top) Schematic of the operation. (bottom) Path of dislocations in the combination NAND gate. Inactive swelling clusters are indicated by a dashed outline. The output zone is shown with a dotted rectangle. Particles are colored by D^2_{min} to highlight dislocation paths.

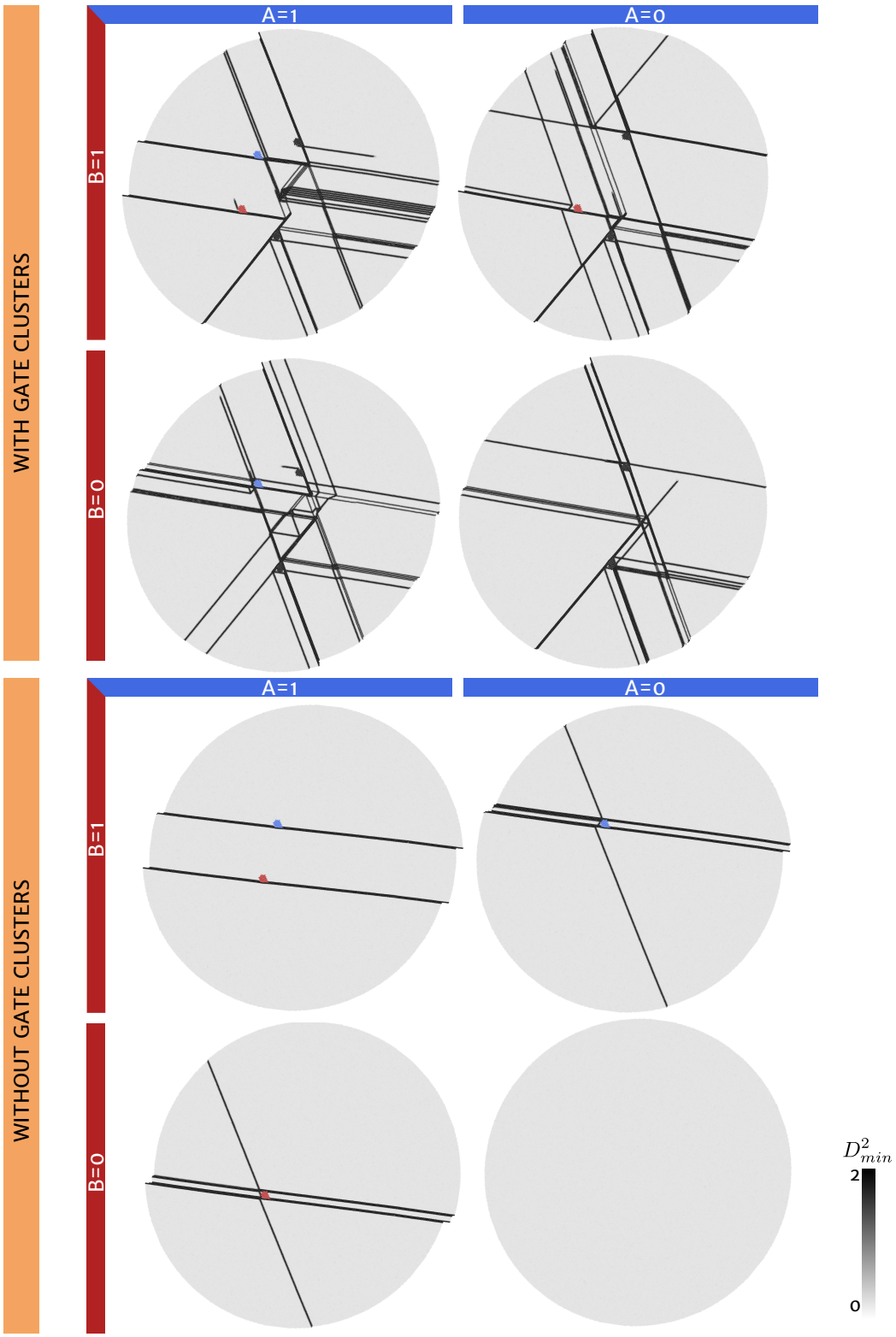


Figure 4.7. Whole-crystallite view comparing effect of input clusters without AND gate. (top) Truth table showing deformation of the entire crystallite with operation of the AND gate. (bottom) Truth table of only the input clusters acting without the AND gate. Particles are colored by D^2_{min} to highlight dislocation paths. Since dislocations deform the crystallite and the D^2_{min} highlights particles moved by dislocation passage, the darker particles in the image guide the eye to where the crystallite surface is deformed.

4.4 Discussion

We provided a new way to think of dislocations as information carriers. Under the constraint of left to right operation, we proposed a realizable implementation of dislocation logic using clusters of swelling particles in a shear field. Our AND gate, NOT gate, and NAND gate show how controlled dislocation reactions can be used to achieve basic logic operations. If coupled with a cluster of sensing, size-changing particles, the input to the gate could be cued by an environmental stimulus, such as light, heat, or pH. This work provides an opportunity to make the entire sense-compute-act loop with dislocations.

Current implementations of topological logic focus on nematic defects in active nematic liquid crystals, are also demonstrated in simulation, yet do not show the sequencing of multiple gates [67, 68]. Encoding logic into materials has been studied for simulations of disclinations in active nematic liquid crystals. For example, in simulation in a 2D system, the passage of a defect can control the path of another defect through patterned high activity regions [67]. Again in simulations, on the surface of a sphere, the interaction of disclination positions with an external field can encode logic gates [68]. Those methods do not have a way to carry the output of one gate to the next. Our work showing how the output of one gate can be fed into another is a first for logic in defects in soft matter systems.

There are several limitations to this work. In our scheme, dislocation motion can serve as information transmission, but it is difficult to synchronize the action of multiple gates. In experiment, perhaps projected light patterns could be used to swell the internal particle clusters in the proper sequence. While we use a clock signal for the gate that is the same as the swelling input signal, when used in a sensing robot, the clock would have to operate separately from the inputs. The arrival of a $(1, 0)$ dislocation means that True is output, but it's less obvious when to register the absence of a dislocation as a False signal, rather than a True signal that has not yet arrived. We must use timing to verify the "non-arrival" of a dislocation to mean False. Other logic systems use the absence of signal to indicate

False, for signals made of a propagating reaction front [89], growth of slime molds [90], or bubbles in microfluidic channels [55]. If deployed in a colloidal robot, there needs to be a way to represent False besides the non-arrival of a True signal.

The use of globally-imposed shear to move dislocations constrains the realm of applicability, yet provides an additional knob that can control the speed of the operation or even pause and reverse it. The shear slowly rotates the crystallite, which means that after some time, the dislocations on the specified glide planes will no longer respond as designed. Varying the shear magnitude and direction over time would open new design possibilities. For example, reversing the shear reverses the glide direction of every dislocation. Coordinating the shear direction with the swelling cycles could allow inputs and outputs to be on the same side of the logic gate.

Because the total Burgers vector is conserved, any bounding box, including the input clusters or even the whole gate must "emit" a total $\vec{0}$ Burgers vector. The problem with this can appear in our NAND gate, where extra dislocations from the AND gate can glide through the NOT gate and appear as an overall output. It is possible to design voids into the crystallite to capture extraneous dislocations so as to isolate the gates from each other.

In this work, we chose a left-to-right constraint to demonstrate sequencing of dislocation logic gates. Depending on the target application of dislocation logic, different dislocation recombinations could be designed, and the requisite swelling clusters set up to enact the logic. The biggest constraint is the choice to use left to right transmission. Choosing different constraints could yield different designs for carrying out dislocation computation, which could be applied to other system configurations. For example, dislocations pre-embedded into the crystal could allow for redirection of dislocations in a predefined way. We demonstrated a concept that should be adapted to other scenarios.

CHAPTER 5

Conclusion and Outlook

In this thesis, we established design rules for actuating and controlling colloidal crystals, opening up new paths for achieving robotic functions in crystalline materials.

Chapter 3 illuminates ways to control dislocation formation around clusters of size-changing particles. By controlling corner angles and side lengths of the cluster, dislocations can be formed along targeted glide planes. At a certain swelling threshold, dislocations emit from acute ($60°$) corners of the shape, which select glide planes that emit dislocations. A rule of thumb from Chapter 3 is that particles swelling 20% is enough to create useful dislocations. Individual sides can be shortened to below the length threshold to further restrict the emission of dislocations to the desired glide planes. One way of effectively shortening a side is to remove alternating particles ("perforating"). These design rules formed the foundation of Chapter 4.

Chapter 4 demonstrated a way to use the interactions between dislocations to encode logical operations. If we see dislocation motion as information transfer, then dislocation interactions are a form of information processing. Harnessing interactions for computation required mapping them to Boolean logic. We identified the $(1, 0)$ dislocation along specified glide planes with logical True. We fixed inputs to be from the left and outputs to be towards the right, all swept along by a global shear field. We showed how to encode an AND gate, NOT gate, and NAND gate into the motion and interaction of dislocations. These gates behaved correctly upwards of 90% of the time. Input dislocations and dislocations internal

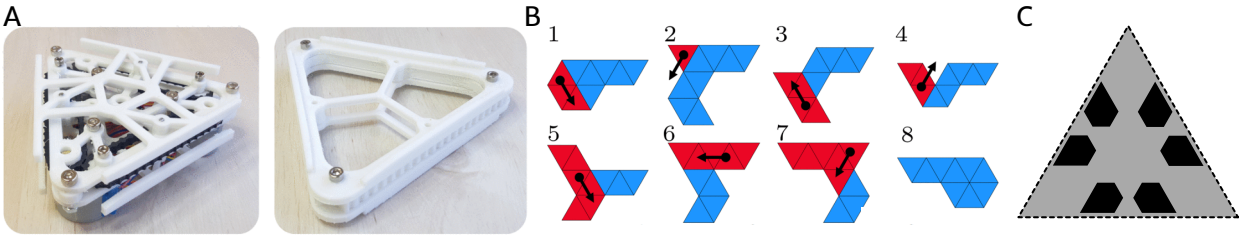


Figure 5.1. Literature design of a robot made of sliding modules. (A) The sliding triangular modules. (B) Sequence of sliding moves (black arrow shows direction) can reconfigure modules one row (red) at a time. From Odem and Medina [91]. (C) A possible design of a crystal module containing swelling clusters to drive the sliding motion, with clusters of swelling particles in black. The large gray triangle would encompass dozens of particles.

to each logic gate were created with the swelling clusters from Chapter 3. This work demonstrated the potential for multiple gates to be chained together. Although we used a Lennard-Jones potential truncated at three particle diameters in this work, the results should apply to any system that can form dislocations.

Within the sense-compute-act paradigm of robotics, this dissertation focused on computation and actuation. In the future, sensing could be implemented for reagents that cause swellable particles to change size. To realize the vision of a colloidal robot [20], passive particles in the current model could be replaced with specialized particles, maintaining the computation and actuation capabilities while adding new ones.

Future work could investigate other cluster swelling mechanisms. For example, asymmetrically swelling particles may provide more tolerance in the patterning of the cluster shape. Swelling in a wave-like pattern would allow for separate control of each half of the dislocation pair formation.

These systems are ripe for experimental implementation, with many kinds of size-changing particles available [84]. The ability to pattern a relatively small number of size-changing particles or selectively target certain particles with heat or light is required to create targeted dislocations.

A theme of this work has been thinking of particles in groups related to their function, such as the cluster of size-changing particles or several clusters acting as a logic gate. A centimeter scale collective robot made from sliding triangular modules is shown in

Figure 5.1A [91]. An algorithm was proposed to decompose a collective reconfiguration into a sequence of sliding motions of the triangular modules. The gliding motion illustrated in Figure 5.1B is like the deformation of our crystallite due to the motion of dislocations along glide planes. To form a crystal gliding module, several clusters could be arranged in a triangle to enclose regions of crystal, such as in Fig. 5.1C.

Some of the problems with dislocation logic are not unlike problems that must be overcome when making traditional integrated circuits. A limitation of the current dislocation logic is the absence of a "False" carrier. As a result, we must resort to external timing to know when a dislocation has *not* arrived. There are natural cycles that could serve as clock ticks, for example: peristalsis (biological pump), heartbeat, circadian rhythm, sun tracking in plants (heliotropic movement), or day-night temperature swings. These could provide timing signals for a crystalline robot deployed in a biological setting. Traditional CMOS logic gates also require precise timing.

Another problem is that wires induce currents in other wires, while here dislocations can leak out from a gate and affect nearby gates. Mitigation techniques may include adding shielding like gaps in the crystal or barriers between gates. A colloidal crystal with a small percentage of dimer particles exhibits slower dislocation motion [92]. To isolate dislocation logic gates from one another, selective regions doped with dimers could serve as barriers for extraneous dislocations.

Breaking out of flat space could also enable new reactions of dislocations. Curved substrates, like the gyroid, sphere, or tube [93], require a default number of defects, changing the notion of defects from inducing to resolving topological strain. Active clusters in non-Euclidean topologies like the surface of a sphere (positive curvature) or gyroid (negative curvature) behave differently [94]. Different constraints due to the inherent defects could be used to design different recombinations, just as we chose constraints within which to design our dislocation logic scheme.

Future work can investigate the effect of imperfections in the crystallite. In general,

dislocation actuation is more robust than dislocation computation because computation relies on a precise sequence of reactions. Point defects, voids and inclusions, do not have a Burgers vector, so they do not misdirect dislocations. However, dislocations already in the crystal would redirect dislocations. For dislocation actuation, with enough swell-shrink cycles, the desired dislocations should surpass the obstacles and enact their designed shape change. Operating a cluster of swelling particles in a crystal with grain boundaries could be a way to shift the grain boundary, because grain boundaries can be seen as arrays of dislocations. For dislocation logic, these stray dislocations or grain boundaries would react with the logic dislocations and cause incorrect results. Possible methods to improve fault tolerance include counting the result of several operations of the logic gate or running multiple gates in parallel and comparing the results.

The ability to program matter itself has been a longstanding goal of colloidal science, whether called "programmable matter" [4] or "infinitesimal machinery" [15]. We hope that this work will serve to advance the ability of crystalline colloidal matter to actuate and compute.

BIBLIOGRAPHY

[1] "R.U.R. (Rossum's Universal Robots)", in Karel Čapek, *R.U.R. and the Vision of Artificial Life*, edited by Jitka Čejková, trans. by Štěpán S. Šimek (The MIT Press, Jan. 16, 2024), pp. 1–98.

[2] S. C. Glotzer and M. J. Solomon, "Anisotropy of building blocks and their assembly into complex structures", Nature Materials **6**, 557–562 (2007).

[3] M. A. McEvoy and N. Correll, "Materials that couple sensing, actuation, computation, and communication", Science **347**, 1261689 (2015).

[4] T. Toffoli and N. Margolus, "Programmable matter: Concepts and realization", Physica D: Nonlinear Phenomena **47**, 263–272 (1991).

[5] D. Rus and M. Vona, "Crystalline Robots: Self-Reconfiguration with Compressible Unit Modules", Autonomous Robots **10**, 107–124 (2001).

[6] M. Rubenstein, A. Cornejo, and R. Nagpal, "Programmable self-assembly in a thousand-robot swarm", Science **345**, 795–799 (2014).

[7] B. Saintyves, M. Spenko, and H. M. Jaeger, "A self-organizing robotic aggregate using solid and liquid-like collective states", Science Robotics **9**, eadh4130 (2024).

[8] S. Goldstein, J. Campbell, and T. Mowry, "Programmable matter", Computer **38**, 99–101 (2005).

[9] B. Kirby, J. D. Campbell, B. Aksak, P. Pillai, J. F. Hoburg, T. C. Mowry, and S. C. Goldstein, "Catoms: Moving robots without moving parts", in AAAI (robot exhibition) (July 2005), pp. 1730–1.

[10] E. Schweikardt, "Designing modular robots", PhD thesis (Carnegie Mellon University, United States – Pennsylvania, 2009), 90 pp.

[11] S. Li, R. Batra, D. Brown, H.-D. Chang, N. Ranganathan, C. Hoberman, D. Rus, and H. Lipson, "Particle robotics based on statistical mechanics of loosely coupled components", Nature **567**, 361–365 (2019).

[12] Q. Jin, Y. Yang, J. A. Jackson, C. Yoon, and D. H. Gracias, "Untethered Single Cell Grippers for Active Biopsy", Nano Letters **20**, 5383–5390 (2020).

[13] E. W. H. Jager, O. Inganäs, and I. Lundström, "Microrobots for Micrometer-Size Objects in Aqueous Media: Potential Tools for Single-Cell Manipulation", Science **288**, 2335–2338 (2000).

[14] M. Urso, M. Ussia, and M. Pumera, "Smart micro- and nanorobots for water purification", Nature Reviews Bioengineering **1**, 236–251 (2023).

[15] R. Feynman, "Infinitesimal machinery", Journal of Microelectromechanical Systems **2**, 4–14 (1993).

[16] V. B. Koman, P. Liu, D. Kozawa, A. T. Liu, A. L. Cottrill, Y. Son, J. A. Lebron, and M. S. Strano, "Colloidal nanoelectronic state machines based on 2D materials for aerosolizable electronics", Nature Nanotechnology **13**, 819–827 (2018).

[17] M. F. Reynolds, A. J. Cortese, Q. Liu, Z. Zheng, W. Wang, S. L. Norris, S. Lee, M. Z. Miskin, A. C. Molnar, I. Cohen, and P. L. McEuen, "Microscopic robots with onboard digital control", Science Robotics **7**, eabq2296 (2022).

[18] M. Z. Miskin, A. J. Cortese, K. Dorsey, E. P. Esposito, M. F. Reynolds, Q. Liu, M. Cao, D. A. Muller, P. L. McEuen, and I. Cohen, "Electronically integrated, mass-manufactured, microscopic robots", Nature **584**, 557–561 (2020).

[19] M. M. Lassiter, J. Lee, K. Skelil, L. Xu, L. Hanson, W. H. Reinhardt, D. Sylvester, M. Yim, D. Blaauw, and M. Z. Miskin, "Microscopic robots that sense, think, act, and compute", Science Robotics **10**, eadu8009 (2025).

[20] A. T. Liu, M. Hempel, J. F. Yang, A. M. Brooks, A. Pervan, V. B. Koman, G. Zhang, D. Kozawa, S. Yang, D. I. Goldman, M. Z. Miskin, A. W. Richa, D. Randall, T. D. Murphey, T. Palacios, and M. S. Strano, "Colloidal robotics", Nature Materials, 1–10 (2023).

[21] T. Hueckel, G. M. Hocky, J. Palacci, and S. Sacanna, "Ionic solids from common colloids", Nature **580**, 487–490 (2020).

[22] J. Liao, C. Zhu, B. Gao, Z. Zhao, X. Liu, L. Tian, Y. Zeng, X. Zhou, Z. Xie, and Z. Gu, "Multiresponsive Elastic Colloidal Crystals for Reversible Structural Color Patterns", Advanced Functional Materials **29**, 1902954 (2019).

[23] P. F. Damasceno, M. Engel, and S. C. Glotzer, "Predictive Self-Assembly of Polyhedra into Complex Structures", Science **337**, 453–457 (2012).

[24] E. V. Shevchenko, D. V. Talapin, N. A. Kotov, S. O'Brien, and C. B. Murray, "Structural diversity in binary nanoparticle superlattices", Nature **439**, 55–59 (2006).

[25] J. H. Holtz and S. A. Asher, "Polymerized colloidal crystal hydrogel films as intelligent chemical sensing materials", Nature **389**, 829–832 (1997).

[26] Y. Yin, Y. Lu, B. Gates, and Y. Xia, "Template-Assisted Self-Assembly: A Practical Route to Complex Aggregates of Monodispersed Colloids with Well-Defined Sizes, Shapes, and Structures", Journal of the American Chemical Society **123**, 8718–8729 (2001).

[27] T. Xu, F. Soto, W. Gao, R. Dong, V. Garcia-Gradilla, E. Magaña, X. Zhang, and J. Wang, "Reversible Swarming and Separation of Self-Propelled Chemically Powered Nanomotors under Acoustic Fields", Journal of the American Chemical Society **137**, 2163–2166 (2015).

[28] L. Ren, N. Nama, J. M. McNeill, F. Soto, Z. Yan, W. Liu, W. Wang, J. Wang, and T. E. Mallouk, "3D steerable, acoustically powered microswimmers for single-particle manipulation", Science Advances **5**, eaax3084 (2019).

[29] J. Palacci, S. Sacanna, A. P. Steinberg, D. J. Pine, and P. M. Chaikin, "Living Crystals of Light-Activated Colloidal Surfers", Science **339**, 936–940 (2013).

[30] T. Vicsek, A. Czirók, E. Ben-Jacob, I. Cohen, and O. Shochet, "Novel Type of Phase Transition in a System of Self-Driven Particles", Physical Review Letters **75**, 1226–1229 (1995).

[31] Shannon E. Moran, Isaac R. Bruss, Philipp W. A. Schönhöfer, and Sharon C. Glotzer, "Particle anisotropy tunes emergent behavior in active colloidal systems", Soft Matter **18**, 1044–1053 (2022).

[32] M. Agrawal, I. R. Bruss, and S. C. Glotzer, "Tunable emergent structures and traveling waves in mixtures of passive and contact-triggered-active particles", Soft Matter **13**, 6332–6339 (2017).

[33] S. Ramananarivo, E. Ducrot, and J. Palacci, "Activity-controlled annealing of colloidal monolayers", Nature Communications **10**, 1–8 (2019).

[34] H. Xie, M. Sun, X. Fan, Z. Lin, W. Chen, L. Wang, L. Dong, and Q. He, "Reconfigurable magnetic microrobot swarm: Multimode transformation, locomotion, and manipulation", Science Robotics **4**, eaav8006 (2019).

[35] G. Romeo, A. Fernandez-Nieves, H. M. Wyss, D. Acierno, and D. A. Weitz, "Temperature-Controlled Transitions Between Glass, Liquid, and Gel States in Dense p-NIPA Suspensions", Advanced Materials **22**, 3441–3445 (2010).

[36] C. Ohm, C. Serra, and R. Zentel, "A Continuous Flow Synthesis of Micrometer-Sized Actuators from Liquid Crystalline Elastomers", Advanced Materials **21**, 4859–4862 (2009).

[37] A. Mourran, H. Zhang, R. Vinokur, and M. Möller, "Soft Microrobots Employing Nonequilibrium Actuation via Plasmonic Heating", Advanced Materials **29**, 1604825 (2017).

[38] W. L. Bragg and J. F. Nye, "A dynamical model of a crystal structure", Proceedings of the Royal Society of London. Series A. Mathematical and Physical Sciences **190**, 474–481 (1947).

[39] P. Schall, I. Cohen, D. A. Weitz, and F. Spaepen, "Visualizing dislocation nucleation by indenting colloidal crystals", Nature **440**, 319–323 (2006).

[40] P. Schall, I. Cohen, D. A. Weitz, and F. Spaepen, "Visualization of Dislocation Dynamics in Colloidal Crystals", Science **305**, 1944–1948 (2004).

[41] A. Stukowski, V. V. Bulatov, and A. Arsenlis, "Automated identification and indexing of dislocations in crystal interfaces", Modelling and Simulation in Materials Science and Engineering **20**, 085007 (2012).

[42] V. A. Lubarda, "Dislocation Burgers vector and the Peach–Koehler force: a review", Journal of Materials Research and Technology **8**, 1550–1565 (2019).

[43] B. VanSaders and S. C. Glotzer, "Sculpting crystals one Burgers vector at a time: Toward colloidal lattice robot swarms", Proceedings of the National Academy of Sciences **118**, e2017377118 (2021).

[44] B. VanSaders, "Defect Control via Active Matter for Reconfigurable Colloidal Crystals" (University of Michigan, Ann Arbor, 2019).

[45] P. M. Anderson, J. P. Hirth, J. Lothe, J. P. Hirth, and J. Lothe, *Theory of dislocations*, Third edition. (Cambridge University Press, New York, NY : 2017).

[46] J. E. Curtis, B. A. Koss, and D. G. Grier, "Dynamic holographic optical tweezers", Optics Communications **207**, 169–175 (2002).

[47] D. G. Grier, "A revolution in optical manipulation", Nature **424**, 810–816 (2003).

[48] W. T. M. Irvine, A. D. Hollingsworth, D. G. Grier, and P. M. Chaikin, "Dislocation reactions, grain boundaries, and irreversibility in two-dimensional lattices using topological tweezers", Proceedings of the National Academy of Sciences **110**, 15544–15548 (2013).

[49] F. A. Lavergne, A. Curran, D. G. A. L. Aarts, and R. P. A. Dullens, "Dislocation-controlled formation and kinetics of grain boundary loops in two-dimensional crystals", Proceedings of the National Academy of Sciences **115**, 6922–6927 (2018).

[50] P. T. Korda and D. G. Grier, "Annealing thin colloidal crystals with optical gradient forces", The Journal of Chemical Physics **114**, 7570–7573 (2001).

[51] B. J. Ackerson and P. N. Pusey, "Shear-Induced Order in Suspensions of Hard Spheres", Physical Review Letters **61**, 1033–1036 (1988).

[52] W. Li, Y. Peng, Y. Zhang, T. Still, A. G. Yodh, and Y. Han, "Shear-assisted grain coarsening in colloidal polycrystals", Proceedings of the National Academy of Sciences **117**, 24055–24060 (2020).

[53] H. Yasuda, P. R. Buskohl, A. Gillman, T. D. Murphey, S. Stepney, R. A. Vaia, and J. R. Raney, "Mechanical computing", Nature **598**, 39–48 (2021).

[54] D. Horsman, S. Stepney, R. C. Wagner, and V. Kendon, "When does a physical system compute?", Proceedings of the Royal Society A: Mathematical, Physical and Engineering Sciences **470**, 20140182 (2014).

[55] M. Prakash and N. Gershenfeld, "Microfluidic Bubble Logic", Science **315**, 832–835 (2007).

[56] T. C. Hull and I. Zakharevich, *Flat origami is Turing Complete*, (Mar. 2, 2024) `http://arxiv.org/abs/2309.07932`, pre-published.

[57] D. J. Preston, P. Rothemund, H. J. Jiang, M. P. Nemitz, J. Rawson, Z. Suo, and G. M. Whitesides, "Digital logic for soft devices", Proceedings of the National Academy of Sciences **116**, 7750–7759 (2019).

[58] M. Agrawal and S. C. Glotzer, *Muscle-inspired flexible mechanical logic architecture for colloidal robotics*, (Dec. 16, 2020) `http://arxiv.org/abs/2012.09345`, pre-published.

[59] E. Fredkin and T. Toffoli, "Conservative logic", International Journal of Theoretical Physics **21**, 219–253 (1982).

[60] T. Toffoli, "Reversible computing", in Automata, Languages and Programming, edited by J. de Bakker and J. van Leeuwen (1980), pp. 632–644.

[61] N. Tanjeem, K. M. Kreienbrink, and R. C. Hayward, "Modulating photothermocapillary interactions for logic operations at the air–water interface", Soft Matter **20**, 1689–1693 (2024).

[62] C. L. Phillips, E. Jankowski, B. Jyoti Krishnatreya, K. V. Edmond, S. Sacanna, D. G. Grier, D. J. Pine, and S. C. Glotzer, "Digital colloids: reconfigurable clusters as high information density elements", Soft Matter **10**, 7468–7479 (2014).

[63] W. Duan, R. Liu, and A. Sen, "Transition between Collective Behaviors of Micromotors in Response to Different Stimuli", Journal of the American Chemical Society **135**, 1280–1283 (2013).

[64] T. H. Ware, M. E. McConney, J. J. Wie, V. P. Tondiglia, and T. J. White, "Voxelated liquid crystal elastomers", Science **347**, 982–984 (2015).

[65] T. Sanchez, D. T. N. Chen, S. J. DeCamp, M. Heymann, and Z. Dogic, "Spontaneous motion in hierarchically assembled active matter", Nature **491**, 431–434 (2012).

[66] M. Nakamura, L. Chen, S. C. Howes, T. D. Schindler, E. Nogales, and Z. Bryant, "Remote control of myosin and kinesin motors using light-activated gearshifting", Nature Nanotechnology **9**, 693–697 (2014).

[67] R. Zhang, A. Mozaffari, and J. J. de Pablo, "Logic operations with active topological defects", Science Advances **8**, eabg9060 (2022).

[68] Ž. Kos and J. Dunkel, "Nematic bits and universal logic gates", Science Advances **8**, eabp8371 (2022).

[69] J. A. Anderson, J. Glaser, and S. C. Glotzer, "HOOMD-blue: A Python package for high-performance molecular dynamics and hard particle Monte Carlo simulations", Computational Materials Science **173**, 109363 (2020).

[70] J. Glaser, T. D. Nguyen, J. A. Anderson, P. Lui, F. Spiga, J. A. Millan, D. C. Morse, and S. C. Glotzer, "Strong scaling of general-purpose molecular dynamics simulations on GPUs", Computer Physics Communications **192**, 97–107 (2015).

[71] C. L. Phillips, J. A. Anderson, and S. C. Glotzer, "Pseudo-random number generation for Brownian Dynamics and Dissipative Particle Dynamics simulations on GPU devices", Journal of Computational Physics **230**, 7191–7201 (2011).

[72] J. E. Lennard-Jones, "Cohesion", Proceedings of the Physical Society **43**, 461 (1931).

[73] G. Bussi, D. Donadio, and M. Parrinello, "Canonical sampling through velocity rescaling", The Journal of Chemical Physics **126**, 014101 (2007).

[74] S. Ganguly, P. S. Mohanty, P. Schurtenberger, S. Sengupta, and A. Yethiraj, "Contrasting the dynamics of elastic and non-elastic deformations across an experimental colloidal Martensitic transition", Soft Matter **13**, 4689–4697 (2017).

[75] G. Voronoi, "Nouvelles applications des paramètres continus à la théorie des formes quadratiques. Deuxième mémoire. Recherches sur les parallélloèdres primitifs.", Journal für die reine und angewandte Mathematik (Crelles Journal) **1908**, 198–287 (1908).

[76] Alexander Stukowski, "A triangulation-based method to identify dislocations in atomistic models", Journal of the Mechanics and Physics of Solids **70**, 314–319 (2014).

[77] M. L. Falk and J. S. Langer, "Dynamics of viscoplastic deformation in amorphous solids", Physical Review E **57**, 7192–7205 (1998).

[78] A. Stukowski, "Visualization and analysis of atomistic simulation data with OVITO–the Open Visualization Tool", Modelling and Simulation in Materials Science and Engineering **18**, 015012 (2009).

[79] *Atomic strain*, OVITO User Manual 3.14.1 documentation, `https://docs.ovito.org/reference/pipelines/modifiers/atomic_strain.html`.

[80] P. Virtanen, R. Gommers, T. E. Oliphant, M. Haberland, T. Reddy, D. Cournapeau, E. Burovski, P. Peterson, W. Weckesser, J. Bright, S. J. van der Walt, M. Brett, J. Wilson, K. J. Millman, N. Mayorov, A. R. J. Nelson, E. Jones, R. Kern, E. Larson, C. J. Carey, İ. Polat, Y. Feng, E. W. Moore, J. VanderPlas, D. Laxalde, J. Perktold, R. Cimrman, I. Henriksen, E. A. Quintero, C. R. Harris, A. M. Archibald, A. H. Ribeiro, F. Pedregosa, P. van Mulbregt, SciPy 1.0 Contributors, A. Vijaykumar, A. P. Bardelli, A. Rothberg, A. Hilboll, A. Kloeckner, A. Scopatz, A. Lee, A. Rokem, C. N. Woods, C. Fulton, C. Masson, C. Häggström, C. Fitzgerald, D. A. Nicholson, D. R. Hagen, D. V. Pasechnik, E. Olivetti, E. Martin, E. Wieser, F. Silva, F. Lenders, F. Wilhelm, G. Young, G. A. Price, G.-L. Ingold, G. E. Allen, G. R. Lee, H. Audren, I. Probst, J. P. Dietrich, J. Silterra, J. T. Webber, J. Slavič, J. Nothman, J. Buchner, J. Kulick, J. L. Schönberger, J. V. de Miranda Cardoso, J. Reimer, J. Harrington, J. L. C. Rodríguez, J. Nunez-Iglesias, J. Kuczynski, K. Tritz, M. Thoma, M. Newville, M. Kümmerer, M. Bolingbroke, M. Tartre, M. Pak, N. J. Smith, N. Nowaczyk, N. Shebanov, O. Pavlyk, P. A. Brodtkorb, P. Lee, R. T. McGibbon, R. Feldbauer, S. Lewis, S. Tygier, S. Sievert, S. Vigna, S. Peterson, S. More, T. Pudlik, T. Oshima, T. J. Pingel, T. P. Robitaille, T. Spura, T. R. Jones, T. Cera, T. Leslie, T. Zito, T. Krauss, U. Upadhyay, Y. O. Halchenko, and Y. Vázquez-Baeza, "SciPy 1.0: fundamental algorithms for scientific computing in Python", Nature Methods **17**, 261–272 (2020).

[81] V. Ramasubramani, B. D. Dice, E. S. Harper, M. P. Spellings, J. A. Anderson, and S. C. Glotzer, "Freud: A software suite for high throughput analysis of particle simulation data", Computer Physics Communications **254**, 107275 (2020).

[82] H. Kim, J.-H. Kang, Y. Zhou, A. S. Kuenstler, Y. Kim, C. Chen, T. Emrick, and R. C. Hayward, "Light-Driven Shape Morphing, Assembly, and Motion of Nanocomposite Gel Surfers", Advanced Materials **31**, 1900932 (2019).

[83] S. Palagi, A. G. Mark, S. Y. Reigh, K. Melde, T. Qiu, H. Zeng, C. Parmeggiani, D. Martella, A. Sanchez-Castillo, N. Kapernaum, F. Giesselmann, D. S. Wiersma, E. Lauga, and P. Fischer, "Structured light enables biomimetic swimming and versatile locomotion of photoresponsive soft microrobots", Nature Materials **15**, 647–653 (2016).

[84] N. Tanjeem, M. B. Minnis, R. C. Hayward, and C. W. Shields IV, "Shape-Changing Particles: From Materials Design and Mechanisms to Implementation", Advanced Materials **34**, 2105758 (2022).

[85] T. J. White and D. J. Broer, "Programmable and adaptive mechanics with liquid crystal polymer networks and elastomers", Nature Materials **14**, 1087–1098 (2015).

[86] R. M. Amos, J. G. Rarity, P. R. Tapster, T. J. Shepherd, and S. C. Kitson, "Fabrication of large-area face-centered-cubic hard-sphere colloidal crystals by shear alignment", Physical Review E **61**, 2929–2935 (2000).

[87] P.-K. Kao, B. J. VanSaders, S. C. Glotzer, and M. J. Solomon, "Accelerated annealing of colloidal crystal monolayers by means of cyclically applied electric fields", Scientific Reports **11**, 11042 (2021).

[88] F. A. Lavergne, A. Curran, D. G. A. L. Aarts, and R. P. A. Dullens, "Shrinkage mechanisms of grain boundary loops in two-dimensional colloidal crystals", The European Physical Journal B **92**, 142 (2019).

[89] O. Steinbock, P. Kettunen, and K. Showalter, "Chemical Wave Logic Gates", The Journal of Physical Chemistry **100**, 18970–18975 (1996).

[90] A. Adamatzky, "Slime mould processors, logic gates and sensors", Philosophical Transactions of the Royal Society A: Mathematical, Physical and Engineering Sciences **373**, 20140216 (2015).

[91] S. Odem and O. Medina, "A Self-Reconfiguration Algorithm for Sliding Triangular Modular Robots", IEEE Robotics and Automation Letters **9**, 2216–2223 (2024).

[92] S. J. Gerbode, S. H. Lee, C. M. Liddell, and I. Cohen, "Restricted Dislocation Motion in Crystals of Colloidal Dimer Particles", Physical Review Letters **101**, 058302 (2008).

[93] A. Zakharov and D. A. Beller, "Shape multistability in flexible tubular crystals through interactions of mobile dislocations", Proceedings of the National Academy of Sciences **119**, e2115423119 (2022).

[94] P. W. A. Schönhöfer and S. C. Glotzer, "Curvature-controlled geometrical lensing behavior in self-propelled colloidal particle systems", Soft Matter **18**, 8561–8571 (2022).